iScience

CellPress
OPEN ACCESS

Article

Neonatal intake of Omega-3 fatty acids enhances lipid oxidation in adipocyte precursors

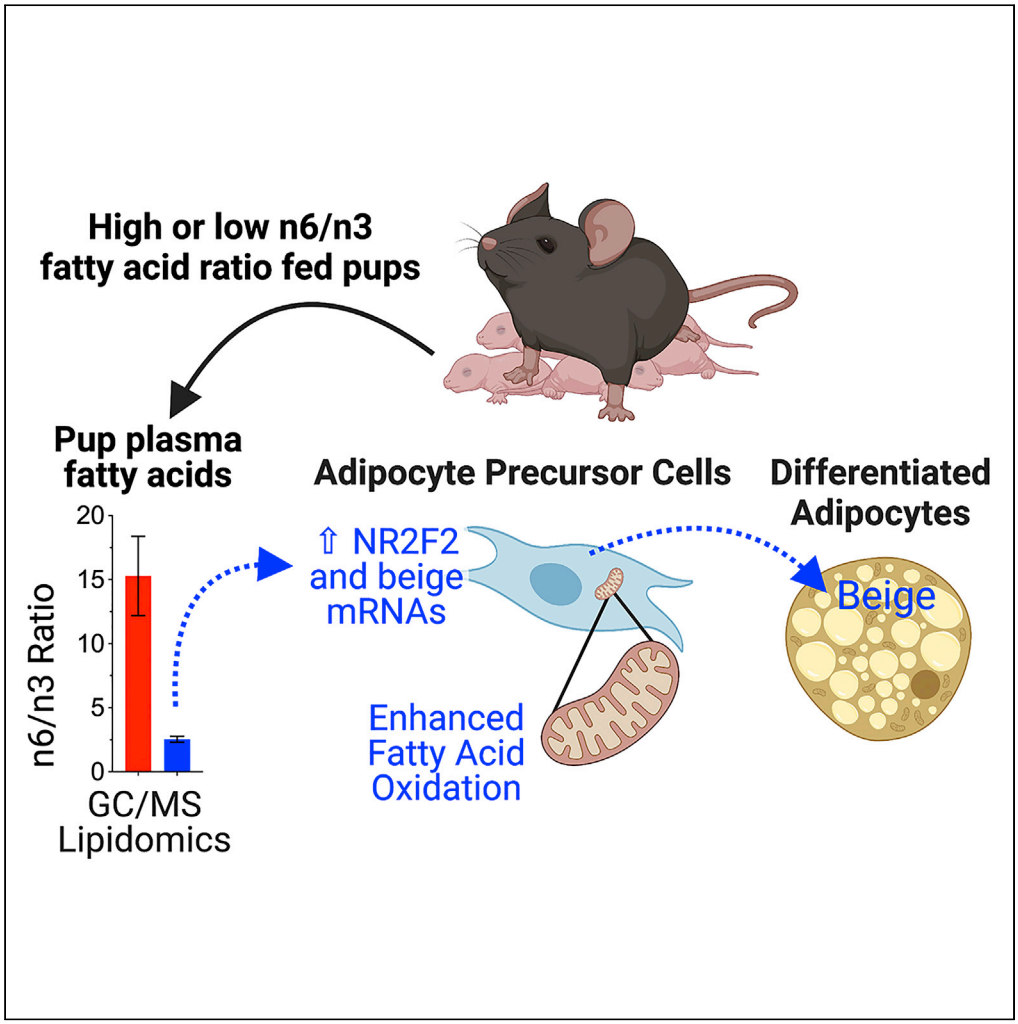

Rohan Varshney, Snehasis Das, G. Devon Trahan, ..., Jacob E. Friedman, Paul S. MacLean, Michael C. Rudolph

michael-rudolph@ouhsc.edu

Highlights

Low n6/n3 FA ratio neonatal intake enhances FA oxidation and beigeing of APCs

Adipogenic regulator NR2F2 is elevated in Low n6/n3 FA exposed APCs *in vivo*

NR2F2 ligand increases the mitochondrial potential and beige mRNAs in APCs *in vitro*

Transcriptomics reveals enriched mitochondrial high APCs during Low n6/n3 FA ratios

Varshney et al., iScience *26*, 105750
January 20, 2023
https://doi.org/10.1016/j.isci.2022.105750

iScience

CellPress
OPEN ACCESS

Article

Neonatal intake of Omega-3 fatty acids enhances lipid oxidation in adipocyte precursors

Rohan Varshney,[1] Snehasis Das,[1] G. Devon Trahan,[2] Jacob W. Farriester,[1] Gregory P. Mullen,[1] Gertrude Kyere-Davies,[1] David M. Presby,[3] Julie A. Houck,[3] Patricia G. Webb,[4] Monika Dzieciatkowska,[5] Kenneth L. Jones,[6] Matthew S. Rodeheffer,[7] Jacob E. Friedman,[1] Paul S. MacLean,[3] and Michael C. Rudolph[1,8,*]

SUMMARY

Establishing metabolic programming begins during fetal and postnatal development, and early-life lipid exposures play a critical role during neonatal adipogenesis. We define how neonatal consumption of a low omega-6 to −3 fatty acid ratio (n6/n3 FA ratio) establishes FA oxidation in adipocyte precursor cells (APCs) before they become adipocytes. *In vivo*, APCs isolated from mouse pups exposed to the low n6/n3 FA ratio had superior FA oxidation capacity, elevated beige adipocyte mRNAs Ppargc1α, Ucp2, and Runx1, and increased nuclear receptor NR2F2 protein. *In vitro*, APC treatment with NR2F2 ligand-induced beige adipocyte mRNAs and increased mitochondrial potential but not mass. Single-cell RNA-sequencing analysis revealed low n6/n3 FA ratio yielded more mitochondrial-high APCs and linked APC NR2F2 levels with beige adipocyte signatures and FA oxidation. Establishing beige adipogenesis is of clinical relevance, because fat depots with energetically active, smaller, and more numerous adipocytes improve metabolism and delay metabolic dysfunction.

INTRODUCTION

Chronic consumption of Western-style diets calorically rich in fat and sugar is associated with non-communicable diseases such as obesity, type 2 diabetes, and cardiovascular diseases. However, for 40 years, it has been known that nutritional exposures during fetal and infant development, derived from maternal diet, can exert long-lasting effects on metabolism, increasing disease risk in youth and across the lifespan.[1–5] For example, infant adiposity has been related to placental lipid trafficking during fetal development,[6] as well as the quantitative fatty acid profile of human milk.[7–9]

In human and rodent models, a high intake of omega-6 (n6) relative to omega-3 (n3) fatty acids (n6/n3 FA ratio) transmitted from mother to offspring accelerates offspring adipose accumulation.[7,10–14] For example, diminished n3 FA in the neonate predicts a higher risk for adiposity at three years old.[10] Consistent with these findings, we observed that increased human milk PUFA n6/n3 ratios positively associate with accelerated infant fat accumulation between two weeks and four months of life.[8,15] In mice, we showed that reducing the n6/n3 PUFA ratio during perinatal development attenuated adipose tissue expansion (ATE) in 14-day-old offspring, producing an adipose morphology consistent with beige adipocytes, attenuated induction of Pparγ2 and its associated lipogenic mRNAs in neonatal subcutaneous white adipose tissue (SWAT), and was associated with adult diet-induced obesity resistance.[16] Taken together, neonatal consumption of a high n6/n3 FA ratio accelerates infant adipose accumulation and predicts adiposity, however, the early molecular mechanisms and operative adipogenic pathways responding to the high n6/n3 FA ratio exposures remain poorly defined.

APCs originate embryonically to facilitate organogenesis of the adipose tissues early in life,[17,18] and developmental adipogenesis and subsequent ATE occurs perinatally in humans and mice.[19,20] Adipogenesis is processive, in that APCs proliferate, give rise to immature adipocytes, and subsequently undergo lipid-filling as mature adipocytes.[21] Accordingly, healthy ATE depends on well-balanced APC proliferation and mature adipocyte hypertrophy (lipid-filling).[22–26] White adipocytes safely harbor dietary fat (FA

[1]Harold Hamm Diabetes Center and Department of Physiology, The University of Oklahoma Health Sciences Center, Oklahoma City, OK, USA

[2]Department of Pediatrics, University of Colorado Denver Anschutz Medical Campus, Aurora, CO, USA

[3]Division of Endocrinology, Metabolism and Diabetes, University of Colorado Anschutz Medical Campus School of Medicine, Aurora, CO, USA

[4]Department of Reproductive Science, University of Colorado Anschutz Medical Campus School of Medicine, Aurora, CO, USA

[5]Department of Biochemistry & Molecular Genetics, University of Colorado Anschutz Medical Campus School of Medicine, Aurora, CO, USA

[6]Department of Cell Biology and Harold Hamm Diabetes Center, The University of Oklahoma Health Sciences Center, Oklahoma City, OK, USA

[7]Department of Molecular, Cellular and Developmental Biology, Department of Comparative Medicine, Yale University, New Haven, CT, USA

[8]Lead contact

*Correspondence: michael-rudolph@ouhsc.edu

https://doi.org/10.1016/j.isci.2022.105750

storage) and arise from the APCs that pattern the form and function of White Adipose Tissue (WAT).[24,26–28] Conversely, the recently characterized "beige" (or "brite") adipocytes arise from the same developmental APC pool as white adipocytes, but remain competent to activate nutrient burning pathways (i.e., FA oxidation).[29] Understanding the adipogenic mechanisms in APCs that lead to differentiation into beige adipocytes is of great clinical relevance because fat depots with smaller, more numerous, and energetically active beige adipocytes improve metabolism and delay insulin resistance.[30–34]

We showed previously that exposure to low n6/n3 PUFA ratios during gestation and lactation facilitated beige adipose morphology, attenuated induction of PPARγ and lipogenic mRNAs and proteins, hypermethylated the PPARγ2 proximal promoter in the SWAT of 14-day-old pups, and the low early-life n6/n3 FA ratio was associated with adult diet-induced obesity resistance and improved glucose clearance.[16] Recent single-cell sequencing findings indicate the potential for numerous APC subtypes, including adipogenesis regulatory,[35] fibrocytes,[36] mural cells,[37,38] progenitors,[21,24,39] and mitochondrial-high APCs.[40] Taken together, these studies suggest a pathway whereby low n6/n3 FA ratio exposure early in life establish obesity resistance by programming APC metabolism or by shifting the cellular diversity of APC subtypes before they give rise to mature adipocytes. We hypothesized that low n6/n3 FA ratio exposures would reveal beige adipocyte metabolic pathways and shift APC subtypes toward single cells with improved FA oxidation mRNA profiles. Here, the low n6/n3 FA ratio exposure was restricted to 10-day of postnatal milk consumption by cross-fostered wildtype pups onto transgenic dams ("*fat-1*") that endogenously drive down the n6/n3 FA ratio in their milk relative to wildtype dams provided the same diet.[16,41,42] This study connects nuclear receptor NR2F2, which is important for adipocyte biology and metabolism,[43,44] with the consumption of low n6/n3 FA ratios during postnatal adipogenesis to promote a pro-beige, lipid burning metabolic phenotype in APCs prior to their functional differentiation into mature adipocytes *in vivo*.

RESULTS

Low n6/n3 serum ratios coincide with reduced circulating adipokines

All wildtype (WT) and *fat-1* experimental dams were provided a corn oil diet rich in n6 polyunsaturated fatty acids (PUFA) at the time of mating. To study postnatal exposure to high or low n6/n3 FA ratio exposures, surrogate WT pups born to non-experimental C57BL/6J mothers on a chow diet were standardized to 6-8 pup litters (experimental neonates) and cross-fostered onto dams that produced milk fat with a high (WT dams) or low (*fat-1* dams) ratio of n6 to n3 PUFA (n6/n3 FA ratio) (Figure 1A). We selected postnatal day 12 for analysis, a time point following the postnatal surge in leptin that is necessary for beige adipocyte development in mice.[45] At postnatal day 12, milk from the dam and neonatal serum total FA composition (TotFA) were quantified by lipid mass spectrometry as previously described.[16] In the milk of Fat-1 dams, long-chain polyunsaturated FA (LC-PUFA), the arachidonic (20:4 n6; AA) to eicosapentaenoic (20:5 n3; EPA) + docosahexaenoic (22:6 n3; DHA) acids, and all PUFA n6/n3 ratios were significantly decreased (Figure 1B), driven primarily by AA, docosatetraenoic acid (22:4 n3), docosapentaenoic acid (22:5 n3), and DHA fatty acids in the composition of the milk. WT offspring consuming the low n6/n3 FA ratio milk had significantly decreased serum n6/n3 ratios for all PUFA, Essential Dietary FA (EFA; 18:2 n6 and 18:3 n3), LC-PUFA, and AA/DHA+EPA (Figure 1B) that were driven by decreases in n6 FA, including AA, docosatetraenoic (22:4 n6), and docosapentaenoic (22:5 n6), with an increase in only the n3 PUFA eicosatrienoic (20:3 n3). No changes in total *de novo* fatty acids (MCFA), total saturated (SatFA), or total monounsaturated FA (MUFA), or in the macronutrient amounts present in the milk (Figure S1A), were observed. Concordant with the decreased n6/n3 FA ratio in neonatal circulation was reduced adipogenesis-related factors acylation stimulating protein (ASP or C3), IGFBP acid labile subunit (ALS), and Retinol-binding protein 4 (RET4, RBP4), and lower Adipsin (ADN, CFD) using unbiased proteomic screens (Table 1).[46–52] In an independent cohort of neonates, circulating levels of the activated form of ASP and RBP4 were significantly reduced (19 and ~5% respectively), while circulating insulin was increased by 32% (Figure 1C). No differences in blood glucose, adiponectin, or leptin were observed (Figure S1B). Together, postnatal consumption of low n6/n3 FA ratio mother's milk effectively reduced the neonatal circulating n6/n3 FA ratio, ASP, Adipsin, ALS, and RBP4 concentrations that are associated with obesity in humans, without changing blood glucose concentration.

Low n6/n3 serum ratio pups have less adiposity and a beige adipose morphology

Body composition of cross-fostered WT litters (males and females combined) was measured by quantitative magnetic resonance as previously described.[16] Following low n6/n3 FA ratio milk consumption,

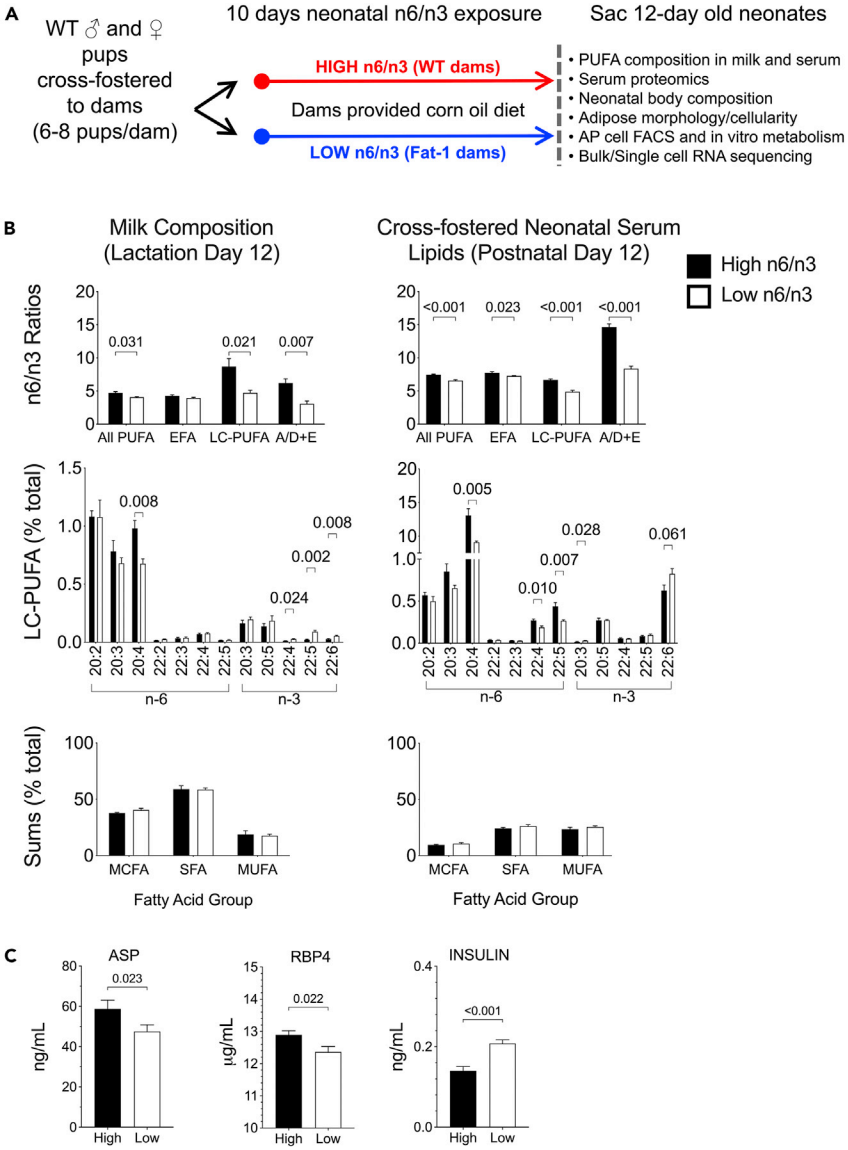

Figure 1. Cross-fostered pups have reduced n6/n3 PUFA ratios, activated Acylation Stimulating Protein (ASP), and Retinol Binding Protein 4 (RBP4) in circulation

(A) Study design to test milk-specific n6/n3 PUFA ratio effects on adipogenesis.

(B) Milk and serum levels of fatty acids and their ratios were quantified by lipid mass spectrometry collected from individual dam's milk (n = 5/group) and the pooled serum of their cross-fostered litters (n = 5 litter dyads per n6/n3 FA ratio exposure) (See also Figure S1).

(C) Circulating factors in PND12 serum that stimulate differential adipogenic responses based on high or low n6/n3 PUFA *in vivo* exposure (See also Data S1). ELISAs for activated Acylation Stimulating Protein (ASP), Retinol Binding Protein 4 (RBP4), and insulin in an independent cohort of cross-fostered PND12 pup sera (n = 5-8 litter dyads per n6/n3 FA ratio exposure). Data are represented as mean ± SEM.

postnatal day 12 neonates with low circulating n6/n3 FA ratios had a 24% (p = 0.022) decrease in body fat mass, without significant changes to lean mass or overall body weight (Figure 2A). Morphologically, subcutaneous white adipose tissue (SWAT) from low n6/n3 consuming pups tended to have a greater proportion of smaller-sized adipocytes relative to the high n6/n3 ratio group (representative histology Figures 2B; p = 0.053, 2D). The dissected SWAT weights were lower, consistent with the observed body fat mass by qMR (p = 0.0019, Figure 2C, n = 6-8 dam/litter dyads per PUFA group). To test whether APC proliferation (hyperplasia) was affected by the n6/n3 FA ratio consumption, deuterated water was given to the dams for

Table 1. Proteomics screen of serum from PND12 wildtype offspring cross-fostered onto high or low n6/n3 milk-producing dams.

Protein Name	Symbol	p value	High ave (SEM)	Low ave (SEM)	Function
Acylation stimulating protein (Complement C3)	ASP	0.0034	1003.3 (46.4)	933.2 (27.9)	Hormone that stimulates adipocyte TAG synthesis and glucose uptake
IGFBP complex acid labile subunit	ALS	0.012	9.1 (1.49)	5.3 (1.36)	Regulation of Insulin-like Growth Factor (IGF) transport and uptake by IGFBPs
Carboxypeptidase Q	CBPQ	0.013	4.8 (0.45)	3 (0.13)	May play a role in the liberation of thyroxine hormone from its thyroglobulin (Tg) precursor
Vitamin D-binding protein	VTDB	0.031	80.7 (9.59)	69.3 (8.16)	Vitamin D transport and storage
Retinol-binding protein 4	RET4	0.01	36 (1.57)	27.5 (3.41)	Retinol transport from the liver to peripheral tissues
Corticosteroid-binding globulin	CBG	0.032	13.2 (1.93)	10.9 (1.12)	Transport protein for glucocorticoids and progestins in the blood
Serum paraoxonase/arylesterase 1	PON1	0.011	22.8 (1.85)	16.3 (1.52)	Enzymatic protection of low-density lipoproteins against oxidative modification
Inactive pancreatic lipase-related protein 1	LIPR1	0.021	5.75 (0.84)	4.9 (0.57)	May function as an inhibitor of dietary triglyceride digestion
Angiotensin-converting enzyme	ACE	0.02	4.2 (0.53)	5.2 (0.57)	Converts angiotensin I to angiotensin II; increases vasoconstrictor activity of angiotensin
Complement C4-B	CO4B	0.00018	49.3 (3.95)	34.8 (3.38)	Non-enzymatic component of C3 and C5 convertases
Complement factor D	CFAD	0.0012	12 (2.02)	7.6 (0.79)	Cleaves factor B, activating the C3bbb complex
Complement factor H	CFAH	0.049	105.7 (4.92)	94.1 (3.95)	Cofactor inactivating C3b by factor I, increases dissociation of the C3 and C5 convertases
Cystatin-C	CYTC	0.012	3.5 (0.34)	2.9 (0.21)	Inhibitor of cysteine proteinases
Alpha-1-antitrypsin 1–2	A1AT2	0.044	14.8 (1.76)	10.8 (1.24)	Inhibitor of serine proteases
Inter-alpha-trypsin inhibitor heavy chain H3	ITIH3	0.048	67.8 (5.53)	74.3 (6.97)	Regulate the localizations, synthesis, and degradation of hyaluronan
Melanocyte protein PMEL	PMEL	0.024	7.2 (0.65)	6.2 (0.69)	The soluble form, ME20-S, could protect tumor cells from antibody-mediated immunity
Extracellular superoxide dismutase [Cu-Zn]	SODE	0.0094	8 (0.57)	6.5 (0.41)	Protect the extracellular space from the toxic effect of reactive oxygen intermediates
Hemopexin	HEMO	0.0051	137.8 (10.5)	152.2 (9.53)	Binds and transports heme to the liver for breakdown and iron recovery
Serotransferrin	TRFE	0.0011	902.8 (14.2)	931.3 (23.1)	Transport of iron from sites of absorption and heme degradation to those of storage
Cathepsin B	CATB	0.028	7.5 (0.84)	6.7 (0.77)	Hydrolysis of proteins with broad specificity for peptide bonds
Plasma protease C1 inhibitor	IC1	0.021	29.7 (2.97)	22.8 (2.15)	Regulates complement activation, blood coagulation, and fibrinolysis

transmission to the neonates via milk. Stable isotope incorporation into the DNA of flow-sorted APCs was quantified.[53–55] Two APC populations, progenitors ($CD24^+$) and the more committed preadipocytes ($CD24^-$) were isolated by flow cytometry as described previously.[56] The overall [^{2}H] molar enrichment was approximately 2.5% (Figure 3A; Δ above the dotted line) and was unchanged by n6/n3 exposure in progenitors, preadipocytes, whole SWAT, or whole blood cell pack, indicating that APC proliferation *in vivo* was unaffected by low n6/n3 FA ratios. A strong trend for a higher fraction of committed adipocyte precursors was observed in flow-sorted APC populations from the low n6/n3 consuming litters, with no change in total cell numbers ($p = 0.06$, Figure 3A panel 3), indicating that a ready pool of preadipocytes exists. When primary APCs were observed by live cell imaging *in vitro*, the % of proliferation was significantly greater in

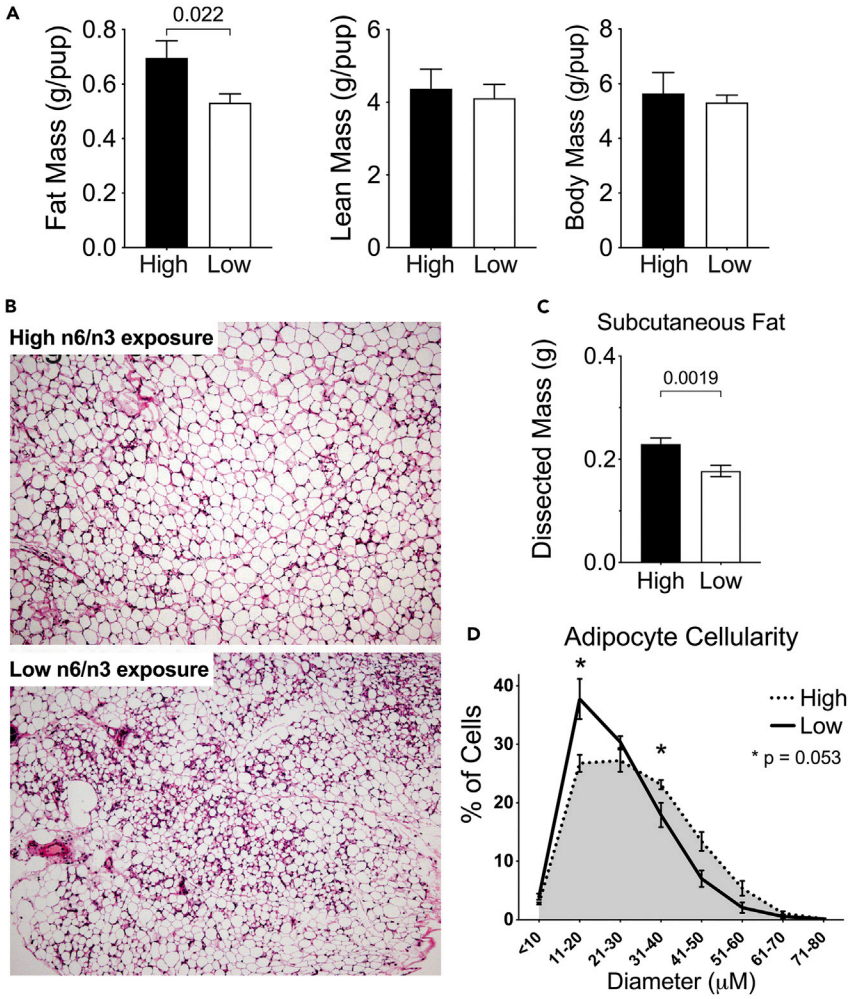

Figure 2. Cross-fostered pups have lower percent body fat and smaller, multilocular adipocyte cellularity

(A) Body fat mass, lean mass, and total body mass of cross-fostered litters containing male and female pups following neonatal adipogenesis in the presence of high or low n6/n3 PUFA in circulation (n = 6-8 litters per n6/n3 FA ratio group; litters standardized to 6-8 pups/litter).

(B) Representative H & E images of SWAT depots following 10 days of exposure to either high or low n6/n3 PUFA ratio.

(C) Scale weights of the dissected SWAT following of 12-day od cross-fostered neonates from high or low n6/n3 PUFA ratio exposure, and D) quantification of the adipocyte cellularity within the SWAT following 10-day of n6/n3 PUFA exposure (n = 5 neonatal SWAT sections from independent dam/litter dyads per n6/n3 group). Data are represented as mean ± SEM.

the high n6/n3 *in vivo* group in both progenitor and preadipocyte APCs (Figure 3B). Once confluent, the % of differentiated cells quantified by neutral lipid staining was lower only in progenitor APCs from the low n6/n3 exposed pups (Figure 3B lower left panel, image at 120 h following adipogenic hormone treatment is representative), indicating *in vivo* programming in progenitor APCs is retained *ex vivo*. Taken together, 10-day of low n6/n3 FA ratio exposure led to pups with less overall SWAT, a shift toward smaller mature adipocytes, with a trend for increased committed $CD24^{-}$preadipocytes, reduced $CD24^{+}$ progenitor differentiation % (*in vitro*), but no significant changes *in vivo* proliferation of APC populations.

In vivo programming by a low n6/n3 ratio enhances adipocyte precursor cell fatty acid oxidation

Given the smaller, multilocular beige-like adipocyte phenotype in low n6/n3 FA ratio consuming neonates, we investigated whether the Sca1+ APCs had an enhanced capacity for mitochondria substrate oxidation. Compared to the high n6/n3 ratio *in vivo* exposure group, APCs from the low n6/n3 group had more robust

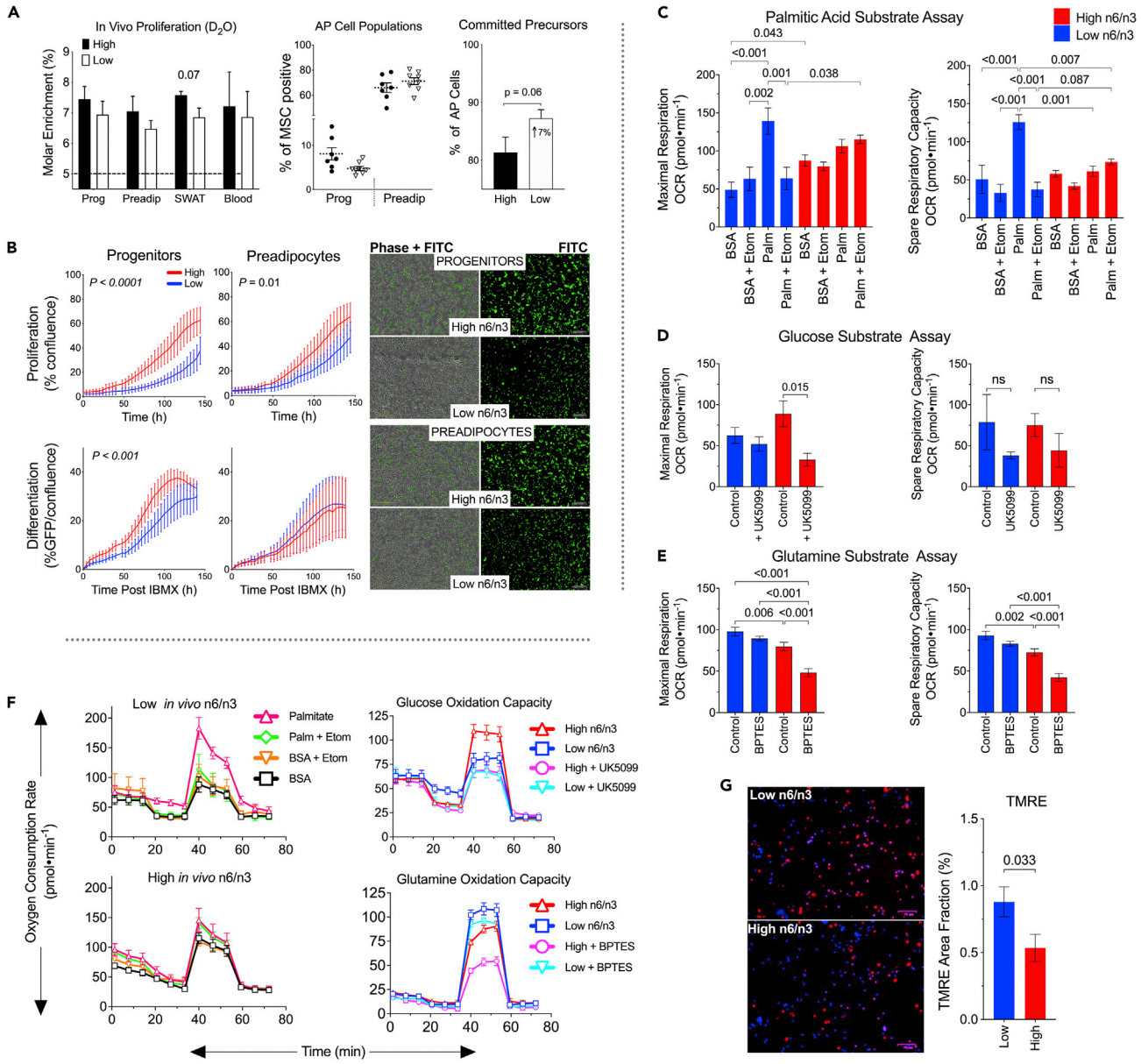

Figure 3. Primary flow-sorted APCs programmed by low n6/n3 FA ratio exposure have reduced white adipose differentiation *in vitro*, greater FA oxidation, and increased mitochondrial potential

(A) Subcutaneous WAT was enzymatically digested to produce a stromal vascular pellet and Fluorescence Assisted Cell Sorting (FACS) was used to isolate $CD24^+$ progenitor from $CD24^-$preadipocyte APCs. Deuterium incorporation into the DNA *in vivo* indicated the rate of APC proliferation is not different, whole SWAT tended to be lower ($p = 0.07$), and a large variance was observed in the whole blood DNA (n = 5-7 litter dyads per n6/n3 FA ratio group; litters standardized to 6-8 pups/litter). APC population analysis indicated no overt difference in $CD24^+$ progenitors and $CD24^-$preadipocytes, and a trend toward the fraction of committed preadipocytes in the low n6/n3 PUFA group (n = 7-8 litter dyads per n6/n3 FA ratio group; litters standardized to 6-8 pups/litter).
(B) Sca-1+ APCs plated for live cell imaging using Incucyte grew more slowly and accumulated less neutral lipid when differentiated to white adipocytes (n = 3 litter dyads per n6/n3 FA ratio group; litters standardized to 6-8 pups/litter), suggesting the potential for a soluble inhibitory factor that curtails white adipocyte differentiation under low n6/n3 *in vivo* programming.
(C-F) Seahorse substrate oxidation assays for primary Sca1+ APCs isolated from low or high n6/n3 ratio exposure (n = 3 litter dyads per n6/n3 FA ratio group; litters standardized to 6-8 pups/litter). Maximal and spare respiration rates from C) exogenous palmitate oxidation, D) glucose, and E) glutamine in low and high n6/n3 *in vivo* programmed primary APCs measured by Seahorse. F) Kinetic data of exogenous palmitate, glucose, and glutamine oxidation assays in C, D, and E.
(G) TMRE live cell mitochondrial potential dye in primary APCs programmed *in vivo* by low and high n6/n3 FA ratio exposure at 24 h post plating (n = 3 litter dyads per n6/n3 FA ratio group; litters standardized to 6-8 pups/litter). Scale bar represents 75 μm. Data are represented as mean ± SEM.

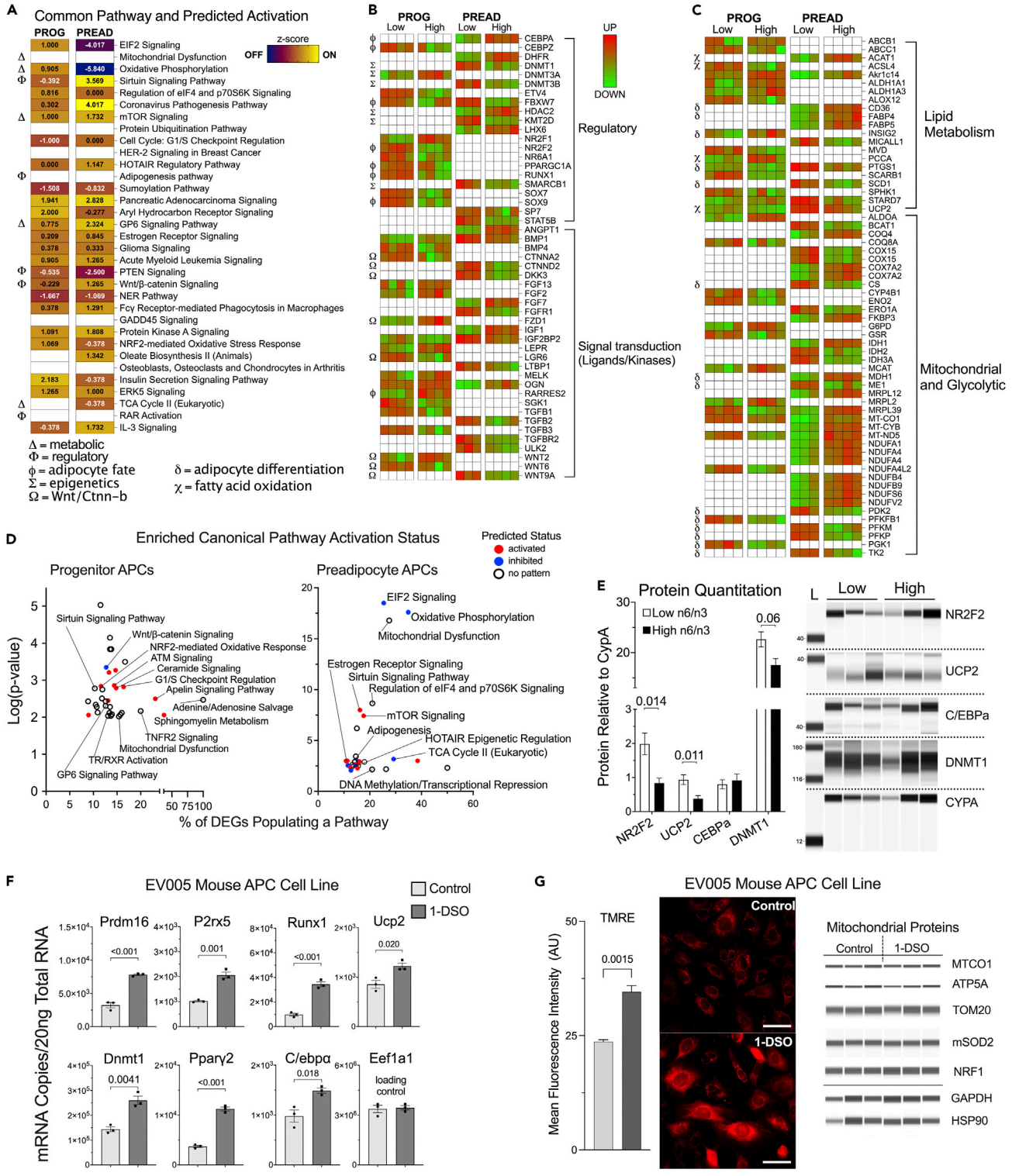

Figure 4. Bulk RNA-seq of flow-sorted APC CD24^{+} progenitors and CD24^{-}preadipocytes reveals transcriptomic signatures for adipogenic, mitochondrial, and energetics pathways by low n6/n3 FA ratios

(A) Differential gene expression by n6/n3 exposure group within either progenitor or preadipocyte APC subtypes was analyzed using comparative analysis in Ingenuity Pathway Analysis. Significantly enriched canonical pathways in common between CD24^{+} progenitor and CD24^{-}preadipocyte APCs were ordered by FDR p value ($\leq$0.01) and colored by the predicted activation *Z* score. Coloring indicates common pathways predicted to be "on" (yellow), "off" (navy), or

Figure 4. *Continued*

"no prediction" (white) due to low n6/n3 exposure. Pathway activation *Z* score values are presented for either APC subtype, and values ≥ 2.0 or ≤ -2.0 are considered significant.

(B) Significantly different genes in either $CD24^+$ progenitor or $CD24^-$preadipocyte relative to the high n6/n3 FA ratio group colored by Log2 fold change and grouped into transcription factor genes (Regulatory) and signal transduction pathway genes (Ligands/Kinases).

(C) Significantly different lipid metabolism, mitochondrial, and glycolytic genes indicating that the low n6/n3 FA ratio changes oxidative capacity potentially through aldehyde dehydrogenases (Aldh1a1 and Aldh1a3), uncoupling protein 2 (Ucp2), citrate synthase (CS), isocitrate dehydrogenase (Idh1 and 2), malic enzyme (Me1), malate dehydrogenase (Mdh1), phosphofructokinases (Pfkm, Pfkp, and Pfkfb1), and transketolase (Tk) (See also Figure S2).

(D) Canonical Pathway enrichment within either $CD24^+$ progenitor or $CD24^-$preadipocyte APCs plotted by the percentage DE-Gs within a pathway (%) by the pathway enrichment significance (-log(p value)) and colored by the predicted pathway activation (*Z* score, >2.0 and < −2.0 was considered significant) (See also Data S3 for all pathways).

(E) Immunoblots for NR2F2, UCP2, C/EBPα, and DNMT1 from all lineage negative, CD29+/CD34+, and Sca1+ APCs isolated by flow cytometry from pooled litters (n = 3 litter dyads per n6/n3 FA ratio group; litters standardized to 6-8 pups/litter).

(F) EVC005 murine APC cell line was treated with and without NR2F2 ligand 1-DSO for 48 h, which induced gene expression of Prdm16, P2rx5, Runx1, Ucp2, Dnmt1, Pparγ2, and C/ebpα.

(G) TMRE live cell mitochondrial potential dye following 48 h of 1-DSO treatment in EVC005 cells, indicating an increased mitochondrial potential. Panels F and G are n = 3 wells per treatment group. Scale bar represents 50 μm. Data are represented as mean ± SEM.

induction of exogenous palmitate oxidation relative to the BSA control (2.85-fold $p < 0.001$), which was sharply inhibited by etomoxir (2.21-fold, $p = 0.002$) (Figure 3C). No significant decrease in maximal respiration was observed between high and low n6/n3 groups (Palm vs. Palm, $p = 0.1$). However, APCs within the high n6/n3 exposure had no etomoxir-dependent reduction in palmitate oxidation (Palm vs. Palm + Etom), which stayed significantly greater in the high n6/n3 relative to the low n6/n3 group (Palm + Etom vs. Palm + Etom, $p = 0.038$) (Figure 3C). Interestingly, a 2.05-fold enhancement in APC spare respiratory capacity (Palm vs. Palm, $p = 0.001$) indicates that APCs exposed to the low n6/n3 ratio had better oxidative capacity than the high n6/n3 group when provided with FA as a mitochondrial fuel source. Neither the low nor high n6/n3 programmed APCs utilized endogenous fatty acids to meet their energy demand (BSA vs. BSA + Etom within group), indicating that isolated APCs do not yet harbor a large endogenous supply of oxidizable lipid. APC programmed *in vivo* were evaluated for glucose (Figure 3D) and glutamine (Figure 3E) oxidative capacities. Only APCs programmed by the high n6/n3 exposure showed strong dependence on glucose (2.71-fold, $p = 0.015$, Control vs. +UK5099 mitochondrial pyruvate carrier inhibitor), and no significant differences were observed in the spare respiratory capacity for glucose oxidation (Figure 3D). Glutamine oxidation was elevated in the low relative to the high n6/n3 group (Control vs. Control, $p = 0.006$, Figure 3E), and only the high n6/n3 group had some dependence on glutamine ($p < 0.001$, Control vs +BPTES glutaminase 1 inhibitor). *In vivo* programming of APCs by low or high n6/n3 ratios did not change basal oxidation of palmitate, glucose, or glutamine (0-15 min, Figure 3F). Consistent with increased mitochondrial potential, the low n6/n3 programmed APCs had 1.65-fold greater tetramethylrhodamine ethyl ester (TMRE) staining in primary APCs ($p = 0.033$) relative to APCs programmed by the high n6/n3 *in vivo* exposure (Figure 3G).

Low n6/n3 FA ratio consumption gives a beige mRNA signature in adipocyte precursor cells

Transcriptional changes leading to enhanced FA oxidation in APC following low n6/n3 exposure were investigated by bulk RNA sequencing of flow-sorted progenitors ($CD24^+$) and preadipocytes ($CD24^-$) isolated from cross-fostered WT pups. Significant differentially expressed gene (DEG) lists were calculated[57] and analyzed for biological pathway/function using the comparison tool from Ingenuity Pathway Analysis, which allows for visualization across multiple analyses, in this case, APC stage and n6/n3 ratio group. DE-Gs regulated by the low relative to high n6/n3 FA ratio returned the predicted biological pathway status for pathways in common between APCs stages (i.e., progenitors and preadipocytes) (Figure 4A). The predicted activation status (yellow = activated, navy = inhibited, or white = no prediction) of common metabolism pathways identified from the DE-Gs included mitochondrial dysfunction (no prediction), oxidative phosphorylation (activated in progenitors; inhibited in preadipocytes), mTOR signaling (activated in both), and TCA cycle II (inhibited in preadipocytes), which is consistent with differences in APC cellular respiration (Figure 4A). Regulatory pathways included Wnt/β-catenin signaling (inhibited in progenitors; activated in preadipocytes), sirtuin signaling (inhibited in progenitors; activated in preadipocytes), mTOR signaling (activated in preadipocytes), adipogenesis (no pattern), PTEN signaling (inhibited in both), Protein Kinase A signaling (activated in preadipocytes), and RAR activation (no pattern). Moreover, Gene Ontology enrichment analysis of the DE-Gs present in preadipocyte APCs indicated that Mitochondrial Organization and Mitochondrial Protein Complex were prominent categories, and Oxidative Phosphorylation and Ribosome were identified by Gene-Concept Network (CNet) plot (Figures S2A and S2B).

Analysis of DE-Gs regulated by low n6/n3 FA ratio in either progenitor or preadipocyte APCs revealed the mRNA control points driving the canonical pathway regulation (Figure 4B). Transcripts known to control adipocyte fate, including CCAAT/enhancer-binding protein alpha (C/ebpα), F box/WD repeat-containing protein 7 (Fbxw7), Nuclear receptor subfamily 2 group F member 2 (Nr2f2), PPAR gamma Coactivator 1 alpha (Ppargc1α), Runt-related transcription factor 1 (Runx1), SRY-Box Transcription Factor 9 (Sox9), and Retinoic acid receptor responder protein 2 (Rarres2), were significantly upregulated in the low n6/n3 FA ratio neonatal APCs. Consistent with epigenetic regulation of adipogenesis, DNA Methyl Transferases 1 and 3B (Dnmt1 and Dnmt3b) were upregulated along with Histone-lysine N-methyltransferase 2D (Kmt2d) and SWI/SNF-related matrix-associated actin-dependent regulator of chromatin subfamily B member 1 (Smarcb1). Additionally, several Wnt/Catenin pathway ligands and modulators are differentially regulated by low n6/n3 FA ratio. Numerous mitochondrial electron transport chain complex I genes were suppressed by low n6/n3 FA ratio in preadipocyte APCs (i.e., NDUFs), while conversely, several TCA enzyme genes (citrate synthase, isocitrate dehydrogenase 2, malic enzyme 1), were upregulated (Figure 4C). It is noteworthy that classic adipocyte differentiation markers Fatty acid binding protein 4 (Fabp4) and Fatty acid translocase (Fat/Cd36) were decreased in the face of sharply upregulated Uncoupling protein 2 (Ucp2) mRNA. Canonical pathway analysis of individual APC subtypes revealed unique pathways activated or inhibited by low n6/n3 exposure. Within progenitors, NRF2-mediated oxidative response, Glucose-6-phosphate (G6P) and Ceramide signaling, Apelin, and TR/RXR activation were enriched (Figure 4D). Within preadipocytes, mTOR signaling, TCA Cycle II, Oxidative phosphorylation, Adipogenesis, and importantly, DNA Methylation and Transcriptional Repression were enriched from DE-Gs in the low relative to the high n6/n3 FA ratio (Figure 4D). In APCs isolated from pooled litters representing three individual dam/litter dyads, protein for NR2F2 ($p = 0.014$) and UCP2 ($p = 0.011$) was significantly increased, while epigenetic regulator DNMT1 tended to be higher ($p = 0.06$), in neonatal APCs from the low n6/n3 FA ratio litters (Figure 4E). Figure S2C contains the top 80 DE-Gs within progenitor and preadipocyte APC subtypes, and Data S3 contains all DE-Gs by n6/n3 FA ratio group within either progenitor or preadipocyte APC subtypes, as well as the full list of enriched canonical pathways. Differential gene expression indicates low n6/n3 ratio regulation for adipogenic mRNAs, including mitochondrial and lipid metabolic enzymes, DNA binding factors, and components of the epigenetic machinery.

Stimulation of adipocyte precursor cell cell line EVC005 with NR2F2 ligand induces beige adipocyte genes and mitochondrial potential

NR2F2 is a nuclear receptor implicated in adipose development and metabolism (reviewed in[43]), whose mRNA was upregulated by low n6/n3 FA ratio *in vivo* exposure in primary APCs. Protein isolated from flow-sorted APCs confirmed a 2.3-fold ($p = 0.014$) increase in NR2F2 protein abundance in the low relative to the high n6/n3 *in vivo* exposed APCs (Figure 4E). The protein level of UCP2 was also significantly increased relative to the high n6/n3 group ($p = 0.011$), and the epigenetic "writer" DNMT1 tended to increase ($p = 0.06$). Using a murine immortalized APC cell line (EVC005), cells were treated for 48 h with the NR2F2 ligand, 1-Deoxysphingosine (m18:1(14Z)) (1-DSO), an atypical, alanine-condensed sphingolipid.[58,59] Following acute NR2F2 treatment with 1-DSO, beige adipocyte mRNAs were significantly increased, including Prdm16, P2rx5, and Runx1 (Figure 4F). Ucp2 and Dnmt1 mRNAs were also significantly increased following NR2F2 treatment ($p = 0.02$ and 0.004, respectively), along with master adipogenic regulators Pparγ2 ($p < 0.001$) and C/ebpα ($p = 0.018$). Levels of Eef1a1 served as a loading control (Figure 4F). Acute stimulation of EVC005 APC cells with 1-DSO also significantly increased TMRE intensity, which accumulates in live cells due to active mitochondrial potential (Figure 4G). Interestingly, no changes in indicators of mitochondrial mass were observed, such as complex IV component MTCO1, complex V component ATP5A, mitochondrial TOM20, and SOD2, or in the mitochondrial biogenesis transcription factor NRF1 (GAPDH and HSP90 as loading controls). Together, NR2F2 protein in primary APCs is increased following low n6/n3 *in vivo* exposure, and acute treatment of EVC005 mouse APC cells with NR2F2 ligand 1-DSO induced expression of beige adipocyte genes and increased mitochondrial potential but not overall mitochondrial mass.

Low n6/n3 FA ratios increase mitochondrial high adipocyte precursor cells and have two pseudotime trajectories

Independent of the bulk RNA-sequencing experiments above, the Sca-1+ population containing both progenitor and preadipocyte APCs was collected and captured for single-cell RNA sequencing using the 10x Genomics platform. APCs exposed to low circulating n6/n3 FA ratios were highly similar in general populations within the UMAP coordinates (colored by n6/n3 group; Figure 5A), indicating the low n6/n3 FA ratios

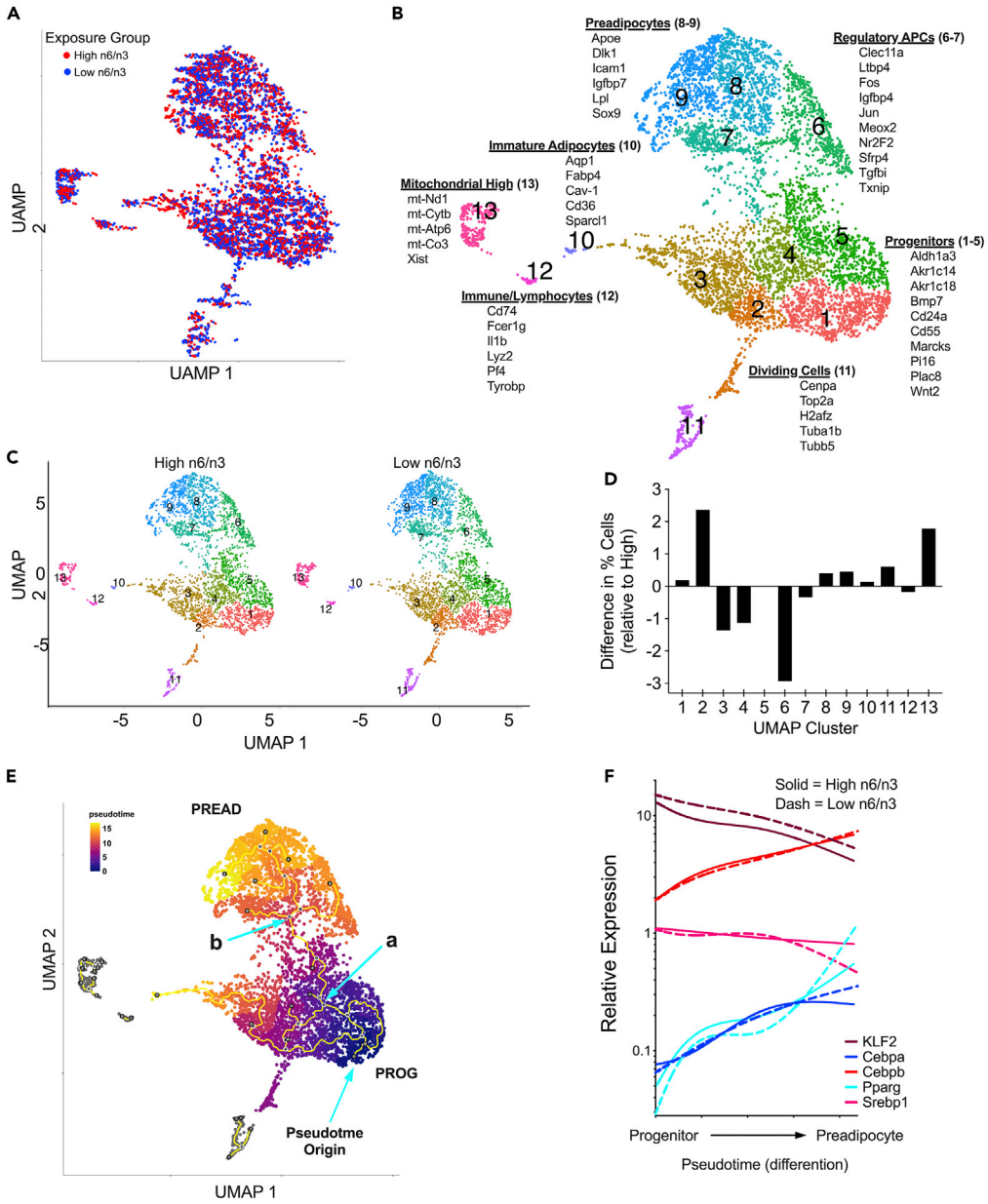

Figure 5. Sca1+ primary APCs single-cell RNA sequencing reveals population differences in APC subtypes

(A) UMAP of the scRNA-seq dataset indicating that exposure to a low n6/n3 ratio produced overlapping populations of primary APCs.

(B) Cluster markers were calculated and principal genes within each cluster were compared to the literature to identify the APC subtypes present (See also Figures S3 and S4, and Data S4).

(C) The distribution of APC subtype within each cluster by n6/n3 FA ratio treatment UMAPs.

(D) The percent difference of APC subtypes within each cluster was calculated (relative to high n6/n3) and indicates populational differences in progenitor cluster 2, regulatory cluster 6, and mitochondrial high cluster 13.

(E) Pseudotime analysis indicated two branchpoints (a and b) that lead to a small pool of immature adipocytes (cluster 10 in panel B), and the other that branches three ways within the regulatory APCs leading to the preadipocyte APCs.

(F) RNA expression trendlines for key adipogenic regulators along pseudotime analysis, indicating a bimodal regulation of Pparγ and C/Ebpα, while adipogenic inhibitor, Klf2, is more highly expressed in the low n6/n3 APCs along pseudotime.

did not produce any discrete subtype of APCs. Cellular identities of several APC subtype populations within the UMAP were observed (Figure 5B), including adipocyte progenitors within clusters 1-5 (Cd24a, Cd55, and Pi16 expression) and preadipocytes within clusters 8 and 9 (Icam1, Dlk-1, Lpl, and Sox9). Interestingly, cluster 13 expressed elevated levels of mitochondrial markers, suggesting that this is an APC population with enhanced cellular respiration. Dividing APCs and immune cell populations (clusters 11 and 12, respectively) comprised a small portion of overall cells (<1%, Figure 5B). Within the Regulatory APC clusters (6 and 7), Clec11a, Ltbp4, Fos, Jun, Srfp4, and Txnip were observed as cluster markers, and three genes known to be expressed in "Adipogenesis regulatory" (Areg) APCs,[35] Nr2f2, Cd142, and Meox2 were expressed in a tight band that spanned clusters 6 and 7 (Figure S3).

When APC clusters were projected onto the UMAP and split by n6/n3 group, the overall density of cells populating each of the 13 clusters was highly similar (Figure 5C). The fraction of cells within each of the individual clusters by the n6/n3 exposure group highlighted subtle population differences within each cluster (Figure 5D), indicating APCs stimulated *in vivo* by low n6/n3 ratios have slight differences in APC populations for clusters 2, 3, 4, 6, and the "mitochondrial" cluster 13 (>1.5% differences, Figure 5D). Because the determination and differentiation of APC progenitor cells into preadipocytes is processive, we analyzed all APCs by pseudotime to evaluate the ordering of each cell by its differentiation status. Pseudotime analysis revealed two individual populations that were furthest along the differentiated path from progenitor cells (Figure 5E). The pseudotime origin was selected to be in cluster 1, and the dividing, immune, and mitochondrial clusters (11, 12, and 13, respectively) were withheld from pseudotime ordering. Inspection of the branchpoints along the pseudotime trajectory indicated two potential adipogenic fate "decisions" are made, one that leads from the progenitors directly to the immature adipocytes (branchpoint "a" leading to cluster 10) and the other within the regulatory APCs leading to the preadipocyte cells (branchpoint "b" within cluster 6 leading to clusters 8 and 9). The relative gene expression for key regulators of adipogenesis along pseudotime was plotted (Figure 5F), indicating that Pparγ mRNA is suppressed by low n6/n3 *in vivo* exposure in more progenitor-like APCs but is greater in preadipocyte APCs. Consistent with this observation is the elevated C/ebpα expression in preadipocyte APCs, while expression of Srebp1 was decreased, and the adipogenesis inhibitor Klf2 mRNA was consistently greater across pseudotime as progenitor APCs differentiate into preadipocytes (Figure 5F). Non-redundant markers within each cluster were plotted by heatmap (Figure S4), and a complete list of all cluster markers ($\geq$1.25 log2 fold change and $\geq$50% expression of all cells) can be found in Data S4. These findings are consistent with single-cell RNA sequencing findings from others, supporting the possibility of independent APC subtypes.[35,36,39,60]

When DE-Gs within a cluster by n6/n3 FA ratio exposure were calculated, important significantly different genes within clusters by n6/n3 group were identified (p-adj <0.05, Figure 6 and Data S5). Consistently, the WNT signaling modulator Secreted frizzled-related protein 4 (Sfrp4) and the lipoprotein lipase inactivation factor Angiopoietin-related protein 4 (Angptl4), were suppressed by low n6/n3 ratios in APC clusters 1, 3, 5, 6, 8, and 9 during adipose development. Conversely, Krueppel-like factors 2 (Klf2, cluster 1) and 4 (Klf4, cluster 3), which are known to inhibit adipogenesis,[61] were induced by the low n6/n3 ratio (UMAPs, Figure S3). DE-Gs were calculated by n6/n3 exposure within all Sca-1+ APCs, and 86 genes were in common with DE-Gs identified from the bulk RNA sequencing experiments (Figure S5), including numerous mitochondrial genes. Together, the low n6/n3 FA ratio established differences in the molecular signatures and the APC subtype diversity (i.e., more mitochondrial-high APCs) before giving rise to differentiated, mature adipocytes.

DISCUSSION

Our previous studies established an early-life adipose morphology consistent with beige adipocytes identified an epigenetic role for n6/n3 FA ratio regulation of subcutaneous white adipose tissue development, and indicated that perinatal exposure to a low n6/n3 FA ratio alone associated with adult resistance to diet-induced obesity.[16] Accordingly, we hypothesized that the adipocyte phenotype established by a low n6/n3 exposure resulted from shifts in the molecular and/or cellular diversity of APC subtype populations present during adipose development toward a beige adipocyte phenotype. Here, we tested for these changes in APC subtypes and mRNA signatures in two ways, first within the lineage negative, MSC+, and Sca1+ APCs present in the stromal vascular fraction using single-cell RNA sequencing analyses, and second, evaluating flow-sorted lineage negative, MSC+, and then further partitioning these populations into APC progenitor (Sca1+/Cd24+) and preadipocyte (Sca1+/Cd24-) populations for bulk transcriptomic profiling. The flow-sorted Sca1+ APCs programmed by the low n6/n3 FA ratio had mitochondrial and cellular respiration mRNA signatures that support the enhanced FA oxidation capacity observed *in vitro* using cellular

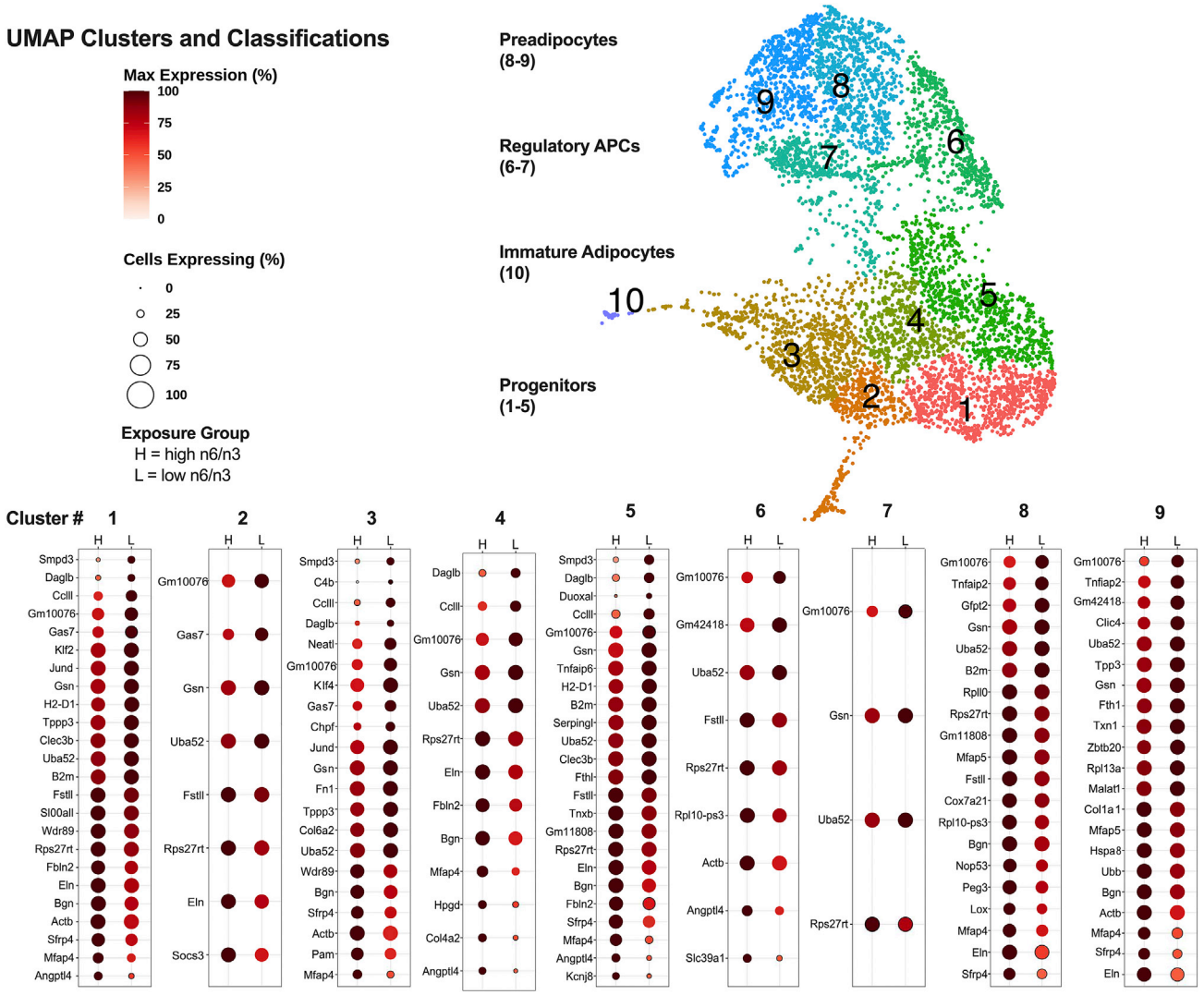

Figure 6. Differential gene expression within clusters by n6/n3 FA ratio group in Sca1+ adipocyte precursors

Genes that were significantly different by n6/n3 exposure were plotted by dot plot for each cluster. The dot size represents the percentage of cells within a cluster expressing a given gene, and the coloring of each dot represents the mean expression of a given cluster relative to the maximum expression for each gene. The canonical Wnt signaling inhibitor Secreted frizzled-related protein 4 (Sfrp4) and an inactivator of lipoprotein lipase Angiopoietin-related protein 4 (Angptl4) were consistently downregulated by low n6/n3 exposure in clusters 1, 3, 5, 6, 8, and 9. Adipogenic transcriptional regulators, Krueppel-like factors 2 and 4, were significantly induced by low n6/n3 exposure but differences were confined to the progenitor clusters (cluster 1 and 3, respectively). No DE-Gs by n6/n3 FA ratio were observed in clusters 10, 11, 13, or 13, which are not shown. (See also Figure S5).

respiration assays. Importantly, the mRNA signatures, APC subtypes, and cellular metabolism were established in APCs prior to the terminal differentiation into mature adipocytes within the fat pad. This finding suggests that distinct mRNA and metabolic features, including elevated levels of NR2F2 and UCP2 protein and predicted the activation of the WNT signaling pathway, are present in neonatal APCs, preceding their functional differentiation into mature adipocytes. Moreover, when the EVC005 APC cell line was treated with nuclear receptor NR2F2 ligand, beige mRNAs and mitochondrial potential were induced, indicating that NR2F2 activation in undifferentiated adipocyte precursor cells may play a key role in establishing mature beige adipocytes. Consistent with improved SWAT adipocyte cellularity, we identified significantly reduced levels of obesity-associated adipokines in neonatal circulation following the low n6/n3 FA ratio consumption. Cumulatively, these findings reveal that neonates consuming a low n6/n3 FA ratio establish putative APC subtypes via cell-intrinsic factors and local paracrine signals, with enhanced oxidative metabolism and attenuated white adipocyte fate.

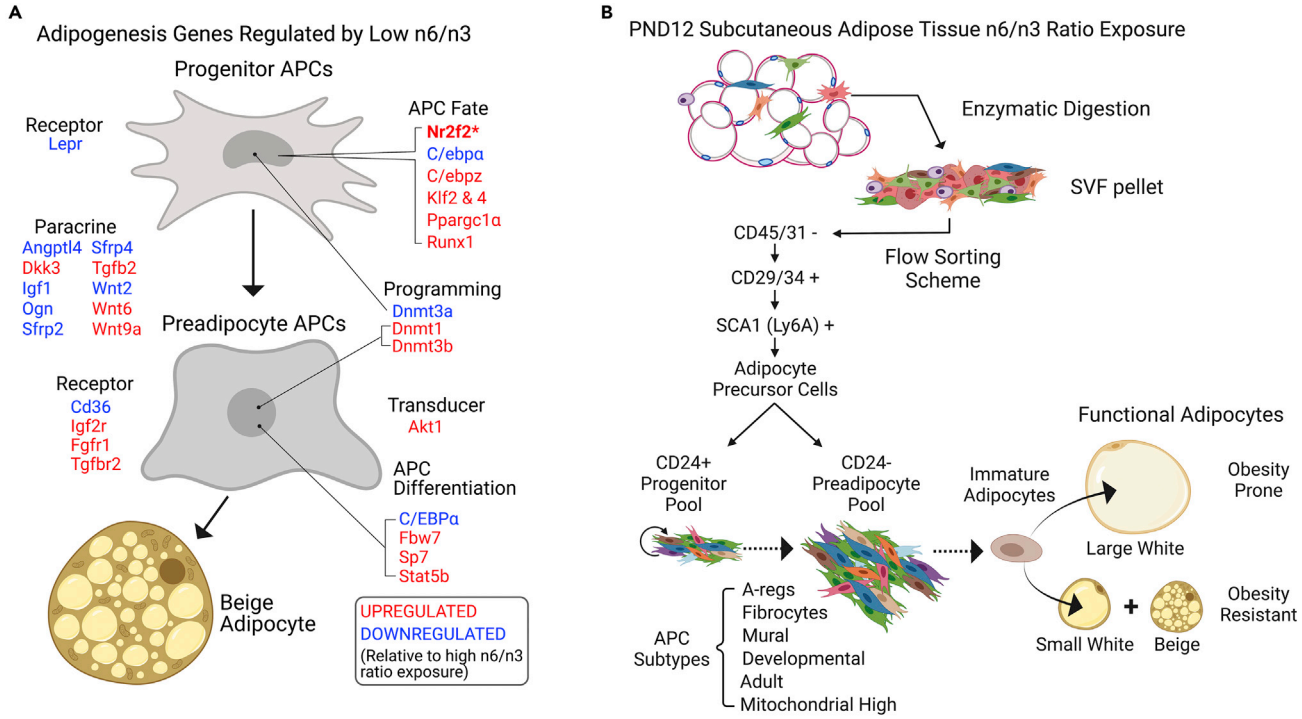

Figure 7. Model of molecular and cellular diversity of APC subtypes regulated by low n6/n3 exposure during postnatal development

(A) Integration of bulk- and scRNA-sequencing observations for adipogenesis-related genes that are up- (red) or down- (blue) regulated *in vivo* by low n6/n3 FA ratio exposure. This transcriptomic signature may establish a cellular metabolism with a greater fatty acid oxidation capacity prior to functional differentiation into a mature adipocyte.

(B) Populations of APC subtypes, such as the balance among regulatory APCs and the number of mitochondrial high APCs, may influence the types of functional mature adipocytes that arise from the APCs. Additionally, the overall proportion of the committed $CD24^{-}$preadipocyte population that expands from the $CD24^{+}$ APCs provides a ready supply of preadipocytes that can functionally differentiate into smaller, more numerous mature adipocytes. Artwork created with BioRender.com.

The combined bulk and single-cell RNA sequencing approach pinpointed APC-intrinsic responses to low n6/n3 FA ratio consumption during postnatal adipogenesis, such as an increased number of mitochondrial-high cells alongside decreased numbers of "Areg" (regulatory) APCs in the single-cell RNA sequencing "snapshot" we examined at postnatal day 12. At present, it is unclear if these changes persist in the mature adipocytes, or if the proportions of APC subtype populations are dynamic over the initial days of life. Overall, neonatal APCs exposed to low n6/n3 FA ratios during this postnatal window have elevated mRNA for beige fat markers Ppargc1α and Runx1, as well as predicted the activation of WNT/β-Catenin signaling pathway due to downregulated Sfrp2 and Sfrp4 concordantly with upregulated Dkk3, Wnt6, and Wnt9a. Moreover, upregulated nuclear receptor Nr2f2, epigenetic regulators Dnmt1 and -3b, and induced transcriptional regulators Klf2 and Klf4 have emerged as possible mediators of low n6/n3 FA ratio response (Figure 7A). Importantly, Nr2f2,[62–64] Sfrp4,[65,66] and Klf2[61,67] are critical factors known to modulate key adipogenic processes that may ultimately impact adipose tissue architecture and function.

Developmental paths toward adipocyte precursor cell subtypes

Pseudotime analysis indicates a branchpoint during the differentiation of Sca1+ APCs in the progenitor populations within cluster 4 (Figure 5) that continues separately to the immature adipocyte population (cluster 10). The alternative trajectory from this first branchpoint leads to the second branchpoint between the regulatory APC populations (clusters 6 and 7) that then continues onward toward the preadipocyte clusters 8 and 9. These findings provide evidence that several adipocyte precursor subtypes established early in life coexist in the SWAT during developmental adipogenesis (Figures 5B and 5D). This observation is consistent with the multitude of elegant *in vivo* lineage tracing studies for APCs that leverage independent strategies to understand the developmental origins of APC subtypes, such as the AdipoTrak system,[60] mosaic labeling using PDGFRα and PDGFRβ[68] (Figure S3), the MuralChaser model,[17,38] and the

Adiponectin-Cre-ErT2.[22,69,70] The literature makes a distinction between populations of adipocyte precursors that originate embryonically to drive adipose tissue organogenesis versus ones that participate in the maintenance of ATE as adults.[17,18] Cumulatively, the complexity of the pseudotime trajectory plotted for all Sca1+ APCs derived from the SWAT of PND12 pups supports a model in which developmental progenitor APC subtypes diverge into Adipogenesis Regulatory,[35] fibrocytes,[36] Mural cells,[37,38] progenitors,[21,24,39] and mitochondrial high APCs,[40] which all may retain plasticity for adopting a beige or white adipocyte phenotype (Figure 7B). Accordingly, beige adipocytes are rich in mitochondria, and there is great interest in how they become established because metabolically active adipose plays a vital role in systemic nutrient homeostasis and energy balance.[33,71]

Metabolic control by developing subcutaneous adipose

The balance of adipocytes within the fat depot during neonatal ATE depends on the proliferation of APCs, processive differentiation into preadipocytes and subsequent hypertrophy of immature adipocytes into lipid-laden mature fat cells. Postnatal exposure to low n6/n3 FA ratio during adipogenesis did not significantly affect the *in vivo* proliferation of cells in the SWAT or significantly change the populations of $CD24^{+}$ and $CD24^{-}$ APCs observed by FACS (Figure 3), despite the significant difference observed in the cellularity and dissected tissue mass (Figure 2). These findings are consistent with our previous work, in that the SWAT of offspring exposed to a combined pre- and postnatal low n6/n3 PUFA ratio was similar in morphology.[16] Together, these findings support a model in which the differences in metabolic programming by low n6/n3 FA ratio consumption establish a more beige-like APC phenotype, which then differentiates into mature adipocytes, thereby driving the reductions in body fat mass observed in the neonates (Figure 2A). In support of a beige fat phenotype are increased levels of the brown fat makers Runx1 and Ppargc1a[72] and differences in mitochondrial gene expression profiles and increased UCP2 (Figure 4), the greater number of mitochondrial high cells populating cluster 13 (Figure 5D), increased dependence on exogenous palmitate oxidation in APCs (Figure 3), the predicted activation of Sirtuin Signaling and mTOR pathways (Figure 4A), and GO enrichment for mitochondrial protein complexes and organization (Figure S2C).

The enhanced mitochondrial respiration of lipids (Figure 3C), in the context of the smaller and multilocular adipocytes (Figure 2), would predict an increased metabolic rate in the neonates if energy intake (i.e., milk consumption) is equivalent among litters, since the milk energy density was equivalent (Figure S1A). Consistent with this concept is the finding that mouse models with selective increases in beige adipocytes have increased energy expenditure, improved insulin sensitivity, and better glucose control when challenged with an obesogenic diet.[33,34,73,74] Recent research indicates that the developing SWAT contains both white and beige APCs that are established in neonates by determination within the committed APC-subtypes, which appear morphologically similar to white adipocytes, but preserve the capacity for burning nutrients.[71,75,76] Interestingly, we observed differences in circulating adipokines (ASP, Adipsin, ALS, RBP4, and a trend for increased Leptin; Figure 1B, Table 1), suggesting that SWAT depots in the neonate secrete a specialized metabolic hormone profile in response to the low n6/n3 FA ratio consumption. It would be interesting to evaluate whether neonatal energy expenditure during growth is impacted by the observed adipose differences.

Long-lasting role of n6/n3 polyunsaturated fatty acid programming

Neonatal consumption of low n6/n3 FA ratios increased Dnmt1 and Dnmt3b mRNA within preadipocyte APCs, and DNMT1 protein tended to be increased within all Sca1+ APCs (Figures 4C and 4E). Importantly, elevated levels of DNMT1 within low n6/n3 FA ratio APCs would be predicted to hypermethylate regions of genes critical to SWAT differentiation,[77] supporting an epigenetic link *in vivo* that we observed previously for the Pparγ locus,[16] thereby providing a link between early life n6/n3 FA consumption and the potential for diet-induced obesity resistance as adults. Whether a low n6/n3 FA ratio leads to epigenetic changes that can alter mitochondria function is unclear, but it is predicted to alter DNA methylated regions of key adipogenic loci of APCs within the developing SWAT. Future studies aim to investigate how adipocyte-specific NR2F2 may interact with epigenetic writers, such as DNMT1, to impart lasting metabolism and healthy adipose, which may protect against obesity in later life. Shifting a "white" differentiation program in favor of "beige" adipocytes via epigenetic regulation would provide the means to connect neonatal exposures with adult obesity protection.

Conclusions

In neonatal mice, lowering the n6/n3 ratio during developmental adipogenesis impacts the overall RNA signatures and APC subtype populations *in vivo*. It establishes an APC-intrinsic metabolism that

preferentially burns fatty acids over storing them. These features are established before differentiation into mature adipocytes, which respond by reducing pro-adipogenic adipokines in the blood.

Limitations of the study

Our study was limited by the broad lipid classification of the n6/n3 FA ratio. Developmental patterning of the neonate is certainly multifactorial, not only regulated by discrete fatty acids (i.e., arachidonic, eicosapentaenoic, or docosahexaenoic acids), but by the hundreds of downstream bioactive lipids taken up by the young during milk consumption.[78–80] For example, lipid activators of brown adipocytes are present in milk, such as the linoleic acid derivative 12,13-diHOME, that may (in part) be responsible for differences in activating adipocyte cellular respiration within the SWAT.[79] Others have identified n3 PUFA as mediators of improved microbiome diversity that, when transplanted into naive hosts, protects against diet-induced obesity and metabolic dysfunction.[81] Altogether, numerous n6-and n3-derived bioactive lipids within neonatal circulation likely act together to establish a metabolic phenotype during developmental adipogenesis and in other metabolic tissues. Although we investigated the neonatal APCs in detail, information regarding whether low n6/n3 FA ratio effects persist in their mature adipocytes within the 12-day-old neonate was not investigated. We were unable to discern sex differences among offspring because litters containing males and females were pooled to attain suitable APC numbers. Finally, we were unable to evaluate whether the low n6/n3 FA ratio impacts the whole animal energy balance, which is the focus of our future studies. Identifying ways to tip the APC determination balance from "*white to beige*" holds great promise in obesity prevention, and nuclear receptor NR2F2 might, in part, mediate the low n6/n3 FA ratio beiging in neonatal APCs.

STAR★METHODS

Detailed methods are provided in the online version of this paper and include the following:

- KEY RESOURCES TABLE
- RESOURCE AVAILABILITY
  - Lead contact
  - Materials availability
  - Data and code availability
- EXPERIMENTAL MODEL AND SUBJECT DETAILS
  - Mouse care
  - Model design
- METHOD DETAILS
  - Body composition
  - Lipid and DNA gas chromatography-mass spectrometry
  - Flow cytometry sorting and analysis
  - Seahorse cellular metabolic assays
  - Tissue culture of mouse APC cell line EVC005
  - qPCR for mouse APC cell line EVC005
  - Live cell TMRE staining
  - Simple Western using JESS
  - Total RNA/DNA isolation and RNA sequencing library preparation
  - Bulk and single-cell RNA-seq data processing and mRNA profiling
  - Offspring plasma proteomics
  - Enzyme-linked immunosorbent assay
- QUANTIFICATION AND STATISTICAL ANALYSES

SUPPLEMENTAL INFORMATION

Supplemental information can be found online at https://doi.org/10.1016/j.isci.2022.105750.

ACKNOWLEDGMENTS

We would like to thank Karen Helm and the University of Colorado Cancer Center Flow Cytometry Core for their expertise in cell sorting and Bifeng Gao and his team at the University of Colorado Genomics Core (both supported by P30CA046934), as well as the Biostatistics and Bioinformatics Shared Resource for primary acquisition and guidance of our sequencing data.

AUTHOR CONTRIBUTIONS

MCR, RV, MSR, JEF, and PSM conceived of this project, designed, and advised the experiments, interpreted the data, and composed the article. RV, SD, GKD, GPM, JWF, JAH, and PGW performed the mouse work, tissue collections, flow sorting, downstream assays, and tissue culture experiments. MCR, GDT, DMP, and KLJ conducted the bulk and single-cell RNA sequencing, processed the raw data, and performed statistical calculations. MD performed the serum proteomics procedure, data acquisition, and processing. All authors contributed to the editing and composition of the article. MCR is the guarantor for this article.

Funding. Support for the authors includes MCR by DK122189-01, DK109079, Ludeman Center for Women's Health Research Pilot Award, NIH/NCATS Colorado CTSA Grant Number UL1 TR002535, and the Oklahoma Center for Adult Stem Cell Research, a program of TSET. Other authors' support includes JEF by DK090964 and DK117418, MSR by DK090489 and DK126447, and PSM by DK48520 and AG062319.

DECLARATION OF INTERESTS

The authors have no conflicts of interest to declare.

INCLUSION AND DIVERSITY

One or more of the authors of this article self-identifies as an underrepresented ethnic minority in their field of research or within their geographical location.

Received: November 30, 2021
Revised: September 26, 2022
Accepted: December 2, 2022
Published: January 20, 2023

REFERENCES

1. Friedman, J.E. (2015). Obesity and gestational diabetes mellitus pathways for programming in mouse, monkey, and man-where do we go next? The 2014 Norbert Freinkel Award Lecture. Diabetes Care *38*, 1402–1411. https://doi.org/10.2337/dc15-0628.

2. Wesolowski, S.R., Kasmi, K.C.E., Jonscher, K.R., and Friedman, J.E. (2017). Developmental origins of NAFLD: a womb with a clue. Nat. Rev. Gastroenterol. Hepatol. *14*, 81–96. https://doi.org/10.1038/nrgastro.2016.160.

3. Koletzko, B., Brands, B., Grote, V., Kirchberg, F.F., Prell, C., Rzehak, P., Uhl, O., and Weber, M.; Early Nutrition Programming Project (2017). Long-term health impact of early nutrition: the power of programming. Ann. Nutr. Metab. *70*, 161–169. https://doi.org/10.1159/000477781.

4. Widdowson, E.M., and McCance, R.A. (1975). A review: new thoughts on growth. Pediatr. Res. *9*, 154–156. https://doi.org/10.1203/00006450-197503000-00010.

5. Rasmussen, K.M. (2001). The "fetal origins" hypothesis: challenges and opportunities for maternal and child nutrition. Annu. Rev. Nutr. *21*, 73–95. https://doi.org/10.1146/annurev.nutr.21.1.73.

6. O'Tierney-Ginn, P.F., Davina, D., Gillingham, M., Barker, D.J.P., Morris, C., and Thornburg, K.L. (2017). Neonatal fatty acid profiles are correlated with infant growth measures at 6 months. J. Dev. Orig. Health Dis. *8*, 474–482. https://doi.org/10.1017/S2040174417000150.

7. Pedersen, L., Lauritzen, L., Brasholt, M., Buhl, T., and Bisgaard, H. (2012). Polyunsaturated fatty acid content of mother's milk is associated with childhood body composition. Pediatr. Res. *72*, 631–636. https://doi.org/10.1038/pr.2012.127.

8. Young, B.E., Levek, C., Reynolds, R.M., Rudolph, M.C., MacLean, P., Hernandez, T.L., Friedman, J.E., and Krebs, N.F. (2018). Bioactive components in human milk are differentially associated with rates of lean and fat mass deposition in infants of mothers with normal vs. elevated BMI. Pediatr. Obes. *13*, 598–606. https://doi.org/10.1111/ijpo.12394.

9. Farahnak, Z., Yuan, Y., Vanstone, C.A., and Weiler, H.A. (2020). Maternal and neonatal red blood cell n-3 polyunsaturated fatty acids inversely associate with infant whole-body fat mass assessed by dual-energy X-ray absorptiometry. Appl. Physiol. Nutr. Metab. *45*, 318–326. https://doi.org/10.1139/apnm-2019-0311.

10. Donahue, S.M.A., Rifas-Shiman, S.L., Gold, D.R., Jouni, Z.E., Gillman, M.W., and Oken, E. (2011). Prenatal fatty acid status and child adiposity at age 3 y: results from a US pregnancy cohort. Am. J. Clin. Nutr. *93*, 780–788. https://doi.org/10.3945/ajcn.110.005801.

11. Muhlhausler, B.S., and Ailhaud, G.P. (2013). Omega-6 polyunsaturated fatty acids and the early origins of obesity. Curr. Opin. Endocrinol. Diabetes Obes. *20*, 56–61. https://doi.org/10.1097/MED.0b013e32835c1ba7.

12. Massiera, F., Barbry, P., Guesnet, P., Joly, A., Luquet, S., Moreilhon-Brest, C., Mohsen-Kanson, T., Amri, E.Z., and Ailhaud, G. (2010). A Western-like fat diet is sufficient to induce a gradual enhancement in fat mass over generations. J. Lipid Res. *51*, 2352–2361. https://doi.org/10.1194/jlr.M006866.

13. Novak, E.M., and Innis, S.M. (2011). Impact of maternal dietary n-3 and n-6 fatty acids on milk medium-chain fatty acids and the implications for neonatal liver metabolism. Am. J. Physiol. Endocrinol. Metab. *301*, E807–E817. https://doi.org/10.1152/ajpendo.00225.2011.

14. Moon, R.J., Harvey, N.C., Robinson, S.M., Ntani, G., Davies, J.H., Inskip, H.M., Godfrey, K.M., Dennison, E.M., Calder, P.C., and Cooper, C.; SWS Study Group (2013). Maternal plasma polyunsaturated fatty acid status in late pregnancy is associated with offspring body composition in childhood. J. Clin. Endocrinol. Metab. *98*, 299–307. https://doi.org/10.1210/jc.2012-2482.

15. Rudolph, M.C., Young, B.E., Lemas, D.J., Palmer, C.E., Hernandez, T.L., Barbour, L.A., Friedman, J.E., Krebs, N.F., and MacLean, P.S. (2017). Early infant adipose deposition is positively associated with the n-6 to n-3 fatty acid ratio in human milk independent of maternal BMI. Int. J. Obes. *41*, 510–517. https://doi.org/10.1038/ijo.2016.211.

16. Rudolph, M.C., Jackman, M.R., Presby, D.M., Houck, J.A., Webb, P.G., Johnson, G.C., Soderborg, T.K., de la Houssaye, B.A., Yang, I.V., Friedman, J.E., and MacLean, P.S. (2018). Low neonatal plasma n-6/n-3 PUFA ratios regulate offspring adipogenic potential and condition adult obesity resistance. Diabetes *67*, 651–661. https://doi.org/10.2337/db17-0890.

17. Hepler, C., Vishvanath, L., and Gupta, R.K. (2017). Sorting out adipocyte precursors and their role in physiology and disease. Genes Dev. *31*, 127–140. https://doi.org/10.1101/gad.293704.116.

18. Ying, T., and Simmons, R.A. (2020). The role of adipocyte precursors in development and obesity. Front. Endocrinol. *11*, 613606. https://doi.org/10.3389/fendo.2020.613606.

19. Poissonnet, C.M., Burdi, A.R., and Garn, S.M. (1984). The chronology of adipose tissue appearance and distribution in the human fetus. Early Hum. Dev. *10*, 1–11.

20. Birsoy, K., Berry, R., Wang, T., Ceyhan, O., Tavazoie, S., Friedman, J.M., and Rodeheffer, M.S. (2011). Analysis of gene networks in white adipose tissue development reveals a role for ETS2 in adipogenesis. Development *138*, 4709–4719. https://doi.org/10.1242/dev.067710.

21. Merrick, D., Sakers, A., Irgebay, Z., Okada, C., Calvert, C., Morley, M.P., Percec, I., and Seale, P. (2019). Identification of a mesenchymal progenitor cell hierarchy in adipose tissue. Science *364*, eaav2501. https://doi.org/10.1126/science.aav2501.

22. Jeffery, E., Wing, A., Holtrup, B., Sebo, Z., Kaplan, J.L., Saavedra-Peña, R., Church, C.D., Colman, L., Berry, R., and Rodeheffer, M.S. (2016). The adipose tissue microenvironment regulates depot-specific adipogenesis in obesity. Cell Metab. *24*, 142–150. https://doi.org/10.1016/j.cmet.2016.05.012.

23. Jeffery, E., Church, C.D., Holtrup, B., Colman, L., and Rodeheffer, M.S. (2015). Rapid depot-specific activation of adipocyte precursor cells at the onset of obesity. Nat. Cell Biol. *17*, 376–385. https://doi.org/10.1038/ncb3122.

24. Berry, R., Jeffery, E., and Rodeheffer, M.S. (2014). Weighing in on adipocyte precursors. Cell Metab. *19*, 8–20. https://doi.org/10.1016/j.cmet.2013.10.003.

25. Church, C.D., Berry, R., and Rodeheffer, M.S. (2014). Isolation and study of adipocyte precursors. Methods Enzymol. *537*, 31–46. https://doi.org/10.1016/B978-0-12-411619-1.00003-3.

26. Berry, R., and Rodeheffer, M.S. (2013). Characterization of the adipocyte cellular lineage in vivo. Nat. Cell Biol. *15*, 302–308. https://doi.org/10.1038/ncb2696.

27. Rodeheffer, M.S., Birsoy, K., and Friedman, J.M. (2008). Identification of white adipocyte progenitor cells in vivo. Cell *135*, 240–249. https://doi.org/10.1016/j.cell.2008.09.036.

28. Hudak, C.S., Gulyaeva, O., Wang, Y., Park, S.M., Lee, L., Kang, C., and Sul, H.S. (2014). Pref-1 marks very early mesenchymal precursors required for adipose tissue development and expansion. Cell Rep. *8*, 678–687. https://doi.org/10.1016/j.celrep.2014.06.060.

29. Townsend, K., and Tseng, Y.H. (2012). Brown adipose tissue: recent insights into development, metabolic function and therapeutic potential. Adipocyte *1*, 13–24. https://doi.org/10.4161/adip.18951.

30. Stenkula, K.G., and Erlanson-Albertsson, C. (2018). Adipose cell size: importance in health and disease. Am. J. Physiol. Regul. Integr. Comp. Physiol. *315*, R284–R295. https://doi.org/10.1152/ajpregu.00257.2017.

31. Laforest, S., Labrecque, J., Michaud, A., Cianflone, K., and Tchernof, A. (2015). Adipocyte size as a determinant of metabolic disease and adipose tissue dysfunction. Crit. Rev. Clin. Lab Sci. *52*, 301–313. https://doi.org/10.3109/10408363.2015.1041582.

32. Longo, M., Zatterale, F., Naderi, J., Parrillo, L., Formisano, P., Raciti, G.A., Beguinot, F., and Miele, C. (2019). Adipose tissue dysfunction as determinant of obesity-associated metabolic complications. Int. J. Mol. Sci. *20*, 2358. https://doi.org/10.3390/ijms20092358.

33. Harms, M., and Seale, P. (2013). Brown and beige fat: development, function and therapeutic potential. Nat. Med. *19*, 1252–1263. https://doi.org/10.1038/nm.3361.

34. Kajimura, S., Spiegelman, B.M., and Seale, P. (2015). Brown and beige fat: physiological roles beyond heat generation. Cell Metab. *22*, 546–559. https://doi.org/10.1016/j.cmet.2015.09.007.

35. Schwalie, P.C., Dong, H., Zachara, M., Russeil, J., Alpern, D., Akchiche, N., Caprara, C., Sun, W., Schlaudraff, K.U., Soldati, G., et al. (2018). A stromal cell population that inhibits adipogenesis in mammalian fat depots. Nature *559*, 103–108. https://doi.org/10.1038/s41586-018-0226-8.

36. Marcelin, G., Ferreira, A., Liu, Y., Atlan, M., Aron-Wisnewsky, J., Pelloux, V., Botbol, Y., Ambrosini, M., Fradet, M., Rouault, C., et al. (2017). A PDGFRalpha-mediated switch toward CD9(high) adipocyte progenitors controls obesity-induced adipose tissue fibrosis. Cell Metab. *25*, 673–685. https://doi.org/10.1016/j.cmet.2017.01.010.

37. Vishvanath, L., Long, J.Z., Spiegelman, B.M., and Gupta, R.K. (2017). Do adipocytes emerge from mural progenitors? Cell Stem Cell *20*, 585–586. https://doi.org/10.1016/j.stem.2017.03.013.

38. Vishvanath, L., MacPherson, K.A., Hepler, C., Wang, Q.A., Shao, M., Spurgin, S.B., Wang, M.Y., Kusminski, C.M., Morley, T.S., and Gupta, R.K. (2016). Pdgfrbeta+ mural preadipocytes contribute to adipocyte hyperplasia induced by high-fat-diet feeding and prolonged cold exposure in adult mice. Cell Metab. *23*, 350–359. https://doi.org/10.1016/j.cmet.2015.10.018.

39. Berry, D.C., Jiang, Y., and Graff, J.M. (2016). Emerging roles of adipose progenitor cells in tissue development, homeostasis, expansion and thermogenesis. Trends Endocrinol. Metab. *27*, 574–585. https://doi.org/10.1016/j.tem.2016.05.001.

40. Scalzo, R.L., Foright, R.M., Hull, S.E., Knaub, L.A., Johnson-Murguia, S., Kinanee, F., Kaplan, J., Houck, J.A., Johnson, G., Sharp, R.R., et al. (2021). Breast cancer endocrine therapy promotes weight gain with distinct adipose tissue effects in lean and obese female mice. Endocrinology *162*, bqab174. https://doi.org/10.1210/endocr/bqab174.

41. Kang, J.X. (2007). Fat-1 transgenic mice: a new model for omega-3 research. Prostaglandins Leukot. Essent. Fatty Acids *77*, 263–267. https://doi.org/10.1016/j.plefa.2007.10.010.

42. Heerwagen, M.J.R., Stewart, M.S., de la Houssaye, B.A., Janssen, R.C., and Friedman, J.E. (2013). Transgenic increase in N-3/n-6 Fatty Acid ratio reduces maternal obesity-associated inflammation and limits adverse developmental programming in mice. PLoS One *8*, e67791. https://doi.org/10.1371/journal.pone.0067791.

43. Ashraf, U.M., Sanchez, E.R., and Kumarasamy, S. (2019). COUP-TFII revisited: its role in metabolic gene regulation. Steroids *141*, 63–69. https://doi.org/10.1016/j.steroids.2018.11.013.

44. Li, L., Xie, X., Qin, J., Jeha, G.S., Saha, P.K., Yan, J., Haueter, C.M., Chan, L., Tsai, S.Y., and Tsai, M.J. (2009). The nuclear orphan receptor COUP-TFII plays an essential role in adipogenesis, glucose homeostasis, and energy metabolism. Cell Metab. *9*, 77–87. https://doi.org/10.1016/j.cmet.2008.12.002.

45. Wu, R., Yu, W., Fu, L., Li, F., Jing, J., Cui, X., Wang, S., Cao, Q., Xue, B., and Shi, H. (2020). Postnatal leptin surge is critical for the transient induction of the developmental beige adipocytes in mice. Am. J. Physiol. Endocrinol. Metab. *318*, E453–E461. https://doi.org/10.1152/ajpendo.00292.2019.

46. Engin, A. (2017). Adiponectin-resistance in obesity. Adv. Exp. Med. Biol. *960*, 415–441. https://doi.org/10.1007/978-3-319-48382-5_18.

47. Jacobo-Cejudo, M.G., Valdés-Ramos, R., Guadarrama-López, A.L., Pardo-Morales, R.V., Martínez-Carrillo, B.E., and Harbige, L.S. (2017). Effect of n-3 polyunsaturated fatty acid supplementation on metabolic and inflammatory biomarkers in type 2 diabetes mellitus patients. Nutrients *9*, 573. https://doi.org/10.3390/nu9060573.

48. Vasilenko, M.A., Kirienkova, E.V., Skuratovskaia, D.A., Zatolokin, P.A., Mironyuk, N.I., and Litvinova, L.S. (2017). The role of production of adipsin and leptin in the development of insulin resistance in patients with abdominal obesity. Dokl. Biochem. Biophys. *475*, 271–276. https://doi.org/10.1134/S160767291704010X.

49. Saleh, J., Al-Maqbali, M., and Abdel-Hadi, D. (2019). Role of complement and complement-related adipokines in regulation of energy metabolism and fat storage. Compr. Physiol. *9*, 1411–1429. https://doi.org/10.1002/cphy.c170037.

50. Olsen, T., and Blomhoff, R. (2020). Retinol, retinoic acid, and retinol-binding protein 4 are differentially associated with cardiovascular disease, type 2 diabetes, and obesity: an overview of human studies. Adv. Nutr. *11*, 644–666. https://doi.org/10.1093/advances/nmz131.

51. Fritton, J.C., Kawashima, Y., Mejia, W., Courtland, H.W., Elis, S., Sun, H., Wu, Y., Rosen, C.J., Clemmons, D., and Yakar, S. (2010). The insulin-like growth factor-1 binding protein acid-labile subunit alters mesenchymal stromal cell fate. J. Biol. Chem. *285*, 4709–4714. https://doi.org/10.1074/jbc.M109.041913.

52. Rasmussen, M.H., Juul, A., Kjems, L.L., and Hilsted, J. (2006). Effects of short-term caloric restriction on circulating free IGF-I, acid-labile subunit, IGF-binding proteins (IGFBPs)-1-4, and IGFBPs-1-3 protease activity in obese subjects. Eur. J. Endocrinol. *155*, 575–581. https://doi.org/10.1530/eje.1.02246.

53. Foletta, V.C., Palmieri, M., Kloehn, J., Mason, S., Previs, S.F., McConville, M.J., Sieber, O.M., Bruce, C.R., and Kowalski, G.M. (2016). Analysis of mammalian cell proliferation and macromolecule synthesis using deuterated water and gas chromatography-mass spectrometry. Metabolites *6*, 34. https://doi.org/10.3390/metabo6040034.

54. Busch, R., Neese, R.A., Awada, M., Hayes, G.M., and Hellerstein, M.K. (2007). Measurement of cell proliferation by heavy water labeling. Nat. Protoc. *2*, 3045–3057. https://doi.org/10.1038/nprot.2007.420.

55. Voogt, J.N., Awada, M., Murphy, E.J., Hayes, G.M., Busch, R., and Hellerstein, M.K. (2007). Measurement of very low rates of cell proliferation by heavy water labeling of DNA and gas chromatography/pyrolysis/isotope ratio-mass spectrometric analysis. Nat. Protoc. *2*, 3058–3062. https://doi.org/10.1038/nprot.2007.421.

56. Zwick, R.K., Rudolph, M.C., Shook, B.A., Holtrup, B., Roth, E., Lei, V., Van Keymeulen, A., Seewaldt, V., Kwei, S., Wysolmerski, J., et al. (2018). Adipocyte hypertrophy and lipid dynamics underlie mammary gland remodeling after lactation. Nat. Commun. *9*, 3592. https://doi.org/10.1038/s41467-018-05911-0.

57. Presby, D.M., Checkley, L.A., Jackman, M.R., Higgins, J.A., Jones, K.L., Giles, E.D., Houck, J.A., Webb, P.G., Steig, A.J., Johnson, G.C., et al. (2019). Regular exercise potentiates energetically expensive hepatic de novo lipogenesis during early weight regain. Am. J. Physiol. Regul. Integr. Comp. Physiol. *317*, R684–R695. https://doi.org/10.1152/ajpregu.00074.

58. Wang, T., Wang, Z., de Fabritus, L., Tao, J., Saied, E.M., Lee, H.J., Ramazanov, B.R., Jackson, B., Burkhardt, D., Parker, M., et al. (2021). 1-deoxysphingolipids bind to COUP-TF to modulate lymphatic and cardiac cell development. Dev. Cell *56*, 3128–3145.e15. https://doi.org/10.1016/j.devcel.2021.10.018.

59. Steiner, R., Saied, E.M., Othman, A., Arenz, C., Maccarone, A.T., Poad, B.L.J., Blanksby, S.J., von Eckardstein, A., and Hornemann, T. (2016). Elucidating the chemical structure of native 1-deoxysphingosine. J. Lipid Res. *57*, 1194–1203. https://doi.org/10.1194/jlr.M067033.

60. Jiang, Y., Berry, D.C., Tang, W., and Graff, J.M. (2014). Independent stem cell lineages regulate adipose organogenesis and adipose homeostasis. Cell Rep. *9*, 1007–1022. https://doi.org/10.1016/j.celrep.2014.09.049.

61. García-Niño, W.R., and Zazueta, C. (2021). New insights of Kruppel-like transcription factors in adipogenesis and the role of their regulatory neighbors. Life Sci. *265*, 118763. https://doi.org/10.1016/j.lfs.2020.118763.

62. Xu, Z., Yu, S., Hsu, C.H., Eguchi, J., and Rosen, E.D. (2008). The orphan nuclear receptor chicken ovalbumin upstream promoter-transcription factor II is a critical regulator of adipogenesis. Proc. Natl. Acad. Sci. USA *105*, 2421–2426. https://doi.org/10.1073/pnas.0707082105.

63. Xie, X., Qin, J., Lin, S.H., Tsai, S.Y., and Tsai, M.J. (2011). Nuclear receptor chicken ovalbumin upstream promoter-transcription factor II (COUP-TFII) modulates mesenchymal cell commitment and differentiation. Proc. Natl. Acad. Sci. USA *108*, 14843–14848. https://doi.org/10.1073/pnas.1110236108.

64. Le Guével, R., Oger, F., Martinez-Jimenez, C.P., Bizot, M., Gheeraert, C., Firmin, F., Ploton, M., Kretova, M., Palierne, G., Staels, B., et al. (2017). Inactivation of the nuclear orphan receptor COUP-TFII by small chemicals. ACS Chem. Biol. *12*, 654–663. https://doi.org/10.1021/acschembio.6b00593.

65. Bukhari, S.A., Yasmin, A., Zahoor, M.A., Mustafa, G., Sarfraz, I., and Rasul, A. (2019). Secreted frizzled-related protein 4 and its implication in obesity and type-2 diabetes. IUBMB Life *71*, 1701–1710. https://doi.org/10.1002/iub.2123.

66. Park, J.R., Jung, J.W., Lee, Y.S., and Kang, K.S. (2008). The roles of Wnt antagonists Dkk1 and sFRP4 during adipogenesis of human adipose tissue-derived mesenchymal stem cells. Cell Prolif. *41*, 859–874. https://doi.org/10.1111/j.1365-2184.2008.00565.x.

67. Wu, Z., and Wang, S. (2013). Role of kruppel-like transcription factors in adipogenesis. Dev. Biol. *373*, 235–243. https://doi.org/10.1016/j.ydbio.2012.10.031.

68. Sun, C., Sakashita, H., Kim, J., Tang, Z., Upchurch, G.M., Yao, L., Berry, W.L., Griffin, T.M., and Olson, L.E. (2020). Mosaic mutant analysis identifies PDGFRalpha/PDGFRbeta as negative regulators of adipogenesis. Cell Stem Cell *26*, 707–721.e5. https://doi.org/10.1016/j.stem.2020.03.004.

69. Moser, C., Straub, L.G., Rachamin, Y., Dapito, D.H., Kulenkampff, E., Ding, L., Sun, W., Modica, S., Balaz, M., and Wolfrum, C. (2021). Quantification of adipocyte numbers following adipose tissue remodeling. Cell Rep. *35*, 109023. https://doi.org/10.1016/j.celrep.2021.109023.

70. Henriques, F., Bedard, A.H., Guilherme, A., Kelly, M., Chi, J., Zhang, P., Lifshitz, L.M., Bellvé, K., Rowland, L.A., Yenilmez, B., et al. (2020). Single-cell RNA profiling reveals adipocyte to macrophage signaling sufficient to enhance thermogenesis. Cell Rep. *32*, 107998. https://doi.org/10.1016/j.celrep.2020.107998.

71. Wu, J., Boström, P., Sparks, L.M., Ye, L., Choi, J.H., Giang, A.H., Khandekar, M., Virtanen, K.A., Nuutila, P., Schaart, G., et al. (2012). Beige adipocytes are a distinct type of thermogenic fat cell in mouse and human. Cell *150*, 366–376. https://doi.org/10.1016/j.cell.2012.05.016.

72. Sun, W., Dong, H., Balaz, M., Slyper, M., Drokhlyansky, E., Colleluori, G., Giordano, A., Kovanicova, Z., Stefanicka, P., Balazova, L., et al. (2020). snRNA-seq reveals a subpopulation of adipocytes that regulates thermogenesis. Nature *587*, 98–102. https://doi.org/10.1038/s41586-020-2856-x.

73. Seale, P., Conroe, H.M., Estall, J., Kajimura, S., Frontini, A., Ishibashi, J., Cohen, P., Cinti, S., and Spiegelman, B.M. (2011). Prdm16 determines the thermogenic program of subcutaneous white adipose tissue in mice. J. Clin. Invest. *121*, 96–105. https://doi.org/10.1172/JCI44271.

74. Boström, P., Wu, J., Jedrychowski, M.P., Korde, A., Ye, L., Lo, J.C., Rasbach, K.A., Boström, E.A., Choi, J.H., Long, J.Z., et al. (2012). A PGC1-alpha-dependent myokine that drives brown-fat-like development of white fat and thermogenesis. Nature *481*, 463–468. https://doi.org/10.1038/nature10777.

75. Xue, R., Lynes, M.D., Dreyfuss, J.M., Shamsi, F., Schulz, T.J., Zhang, H., Huang, T.L., Townsend, K.L., Li, Y., Takahashi, H., et al. (2015). Clonal analyses and gene profiling identify genetic biomarkers of the thermogenic potential of human brown and white preadipocytes. Nat. Med. *21*, 760–768. https://doi.org/10.1038/nm.3881.

76. Shao, M., Wang, Q.A., Song, A., Vishvanath, L., Busbuso, N.C., Scherer, P.E., and Gupta, R.K. (2019). Cellular origins of beige fat cells revisited. Diabetes *68*, 1874–1885. https://doi.org/10.2337/db19-0308.

77. Roh, H.C., Tsai, L.T.Y., Lyubetskaya, A., Tenen, D., Kumari, M., and Rosen, E.D. (2017). Simultaneous transcriptional and epigenomic profiling from specific cell types within heterogeneous tissues in vivo. Cell Rep. *18*, 1048–1061. https://doi.org/10.1016/j.celrep.2016.12.087.

78. Isganaitis, E., Venditti, S., Matthews, T.J., Lerin, C., Demerath, E.W., and Fields, D.A. (2019). Maternal obesity and the human milk metabolome: associations with infant body composition and postnatal weight gain. Am. J. Clin. Nutr. *110*, 111–120. https://doi.org/10.1093/ajcn/nqy334.

79. Wolfs, D., Lynes, M.D., Tseng, Y.H., Pierce, S., Bussberg, V., Darkwah, A., Tolstikov, V., Narain, N.R., Rudolph, M.C., Kiebish, M.A., et al. (2021). Brown fat-activating lipokine 12, 13-diHOME in human milk is associated with infant adiposity. J. Clin. Endocrinol. Metab.

106, e943–e956. https://doi.org/10.1210/clinem/dgaa799.

80. Riederer, M., Wallner, M., Schweighofer, N., Fuchs-Neuhold, B., Rath, A., Berghold, A., Eberhard, K., Groselj-Strele, A., Staubmann, W., Peterseil, M., et al. (2020). Distinct maternal amino acids and oxylipins predict infant fat mass and fat-free mass indices. Arch. Physiol. Biochem. 1–12. https://doi.org/10.1080/13813455.2020.1846204.

81. Bidu, C., Escoula, Q., Bellenger, S., Spor, A., Galan, M., Geissler, A., Bouchot, A., Dardevet, D., Morio, B., Cani, P.D., et al. (2018). The transplantation of omega3 PUFA-altered gut microbiota of fat-1 mice to wild-type littermates prevents obesity and associated metabolic disorders. Diabetes *67*, 1512–1523. https://doi.org/10.2337/db17-1488.

82. Rudolph, M.C., Young, B.E., Jackson, K.H., Krebs, N.F., Harris, W.S., and MacLean, P.S. (2016). Human milk fatty acid composition: comparison of novel dried milk spot versus standard liquid extraction methods. J. Mammary Gland Biol. Neoplasia *21*, 131–138. https://doi.org/10.1007/s10911-016-9365-4.

83. Presby, D.M., Rudolph, M.C., Sherk, V.D., Jackman, M.R., Foright, R.M., Jones, K.L., Houck, J.A., Johnson, G.C., Higgins, J.A., Neufer, P.D., et al. (2021). Lipoprotein lipase overexpression in skeletal muscle attenuates weight regain by potentiating energy expenditure. Diabetes *70*, 867–877. https://doi.org/10.2337/db20-0763.

84. Martin Carli, J.F., Trahan, G.D., Jones, K.L., Hirsch, N., Rolloff, K.P., Dunn, E.Z., Friedman, J.E., Barbour, L.A., Hernandez, T.L., MacLean, P.S., et al. (2020). Single cell RNA sequencing of human milk-derived cells reveals sub-populations of mammary epithelial cells with molecular signatures of progenitor and mature states: a novel, non-invasive framework for investigating human lactation physiology. J. Mammary Gland Biol. Neoplasia *25*, 367–387. https://doi.org/10.1007/s10911-020-09466-z.

STAR★METHODS

KEY RESOURCES TABLE

REAGENT or RESOURCE	SOURCE	IDENTIFIER
Antibodies		
FITC anti-mouse CD45 Monoclonal Antibody	BioLegend	Cat# 103108
PE/Cyanine7 anti-mouse CD31 Monoclonal Antibody	BioLegend	Cat# 102417; RRID: AB_830756
Alexa Fluor® 700 anti-mouse/rat CD29 Monoclonal Antibody	BioLegend	Cat# 102218; RRID: AB_493711
APC anti-mouse CD34 Monoclonal Antibody	BioLegend	Cat# 119310; RRID: AB_1236469
Brilliant Violet 510™ anti-mouse Ly-6A/E (Sca-1) Monoclonal Antibody	BioLegend	Cat# 108129; RRID: AB_2561593
PE anti-mouse CD24 Antibody	BioLegend	Cat# 138504; RRID: AB_10578416
UCP2 (D1O5V) Rabbit Monoclonal Antibody	Cell Signaling	Cat# 89326; RRID: AB_2721818
C/EBPα (D56F10) XP® Rabbit Monoclonal Antibody	Cell Signaling	Cat# 8178; RRID: AB_11178517
TOM20 (D8T4N) Rabbit Monoclonal Antibody	Cell Signaling	Cat# 42406; RRID: AB_2687663
SOD2 (D3X8F) Rabbit Monoclonal Antibody	Cell Signaling	Cat# 13141; RRID: AB_2636921
NRF1 (D9K6P) Rabbit Monoclonal Antibody	Cell Signaling	Cat# 46743; RRID: AB_2732888
HSP90 Rabbit Polyclonal Antibody	Cell Signaling	Cat# 4874; RRID: AB_2121214
GAPDH (D16H11) Rabbit Monoclonal Antibody	Cell Signaling	Cat# 5174; RRID: AB_10622025
OxPhos Rodent WB Antibody Cocktail	ThermoFisher	Cat# 45–8099; RRID: AB_2533835
COUP-TFII (D16C4) Rabbit Monoclonal Antibody	Cell Signaling	Cat# 6434; RRID: AB_11220428
Mouse monoclonal anti-DNMT-1 antibody	Novus Biologicals	Cat# NB100-56519; RRID: AB_2093819
Chemicals, peptides, and recombinant proteins		
TMRE, 2 mM solution in DMSO	Biotium	Cat# 70005
1-Deoxysphingosine	Cayman Chemicals	Cat# 24515
Critical commercial assays		
Quick DNA/RNA MiniPrep Plus Kit	Zymo Research	Cat# D7003
XF Glucose/Pyruvate Oxidation Stress Test Kit	Agilent	Cat# 103673–100
XF Glutamine Oxidation Stress Test Kit	Agilent	Cat# 103674–100
XF Palmitate Oxidation Stress Test Kit	Agilent	Cat# 103693–100
Universal Plus mRNA-SEQ kit	NuGEN/TECAN	Cat# 0520
High Molecular Weight and Total Adiponectin ELISA	ALPCO	Cat# 47-ADPMS-E01
Acylation Stimulating Protein ELISA	MyBioSource	Cat# MBS263213
Complement C3 ELISA	Abcam	Cat# ab157711
Leptin ELISA	R&D	Cat# DY498
Insulin ELISA	Crystal Chem	Cat# 90080
Retinol-Binding Protein 4 ELISA	R&D	Cat# DY3476
Deposited data		
Bulk and Single Cell RNA-seq Raw Data files	This Paper	GEO: GSE155895

(*Continued on next page*)

Continued

REAGENT or RESOURCE	SOURCE	IDENTIFIER
Experimental models: Cell lines		
Mouse Inguinal Adipose SVF Preadipocyte Cell Line	Kerafast	Cat# EVC005; RRID: CVCL_ZD83
Experimental models: Organisms/strains		
Mouse: C57BL/6J	The Jackson Laboratory	RRID:IMSR_JAX:000664
Mouse: C57BL/6-Tg(CAG-fat-1)1Jxk/J	The Jackson Laboratory	RRID:IMSR_JAX:020097
Oligonucleotides		
Prdm16 mouse TaqMan Primer	ThermoFisher Scientific	Cat# Mm00712556_m1
P2rx5 mouse TaqMan Primer	ThermoFisher Scientific	Cat# Mm00473677_m1
Runx1 mouse TaqMan Primer	ThermoFisher Scientific	Cat# Mm01213404_m1
Ucp2 mouse TaqMan Primer	ThermoFisher Scientific	Cat# Mm00627599_m1
Dnmt1 mouse TaqMan Primer	ThermoFisher Scientific	Cat# Mm01151063_m1
Ppar-gamma2 mouse TaqMan Primer	ThermoFisher Scientific	Cat# Mm01184322_m1
C/ebp-alpha mouse TaqMan Primer	ThermoFisher Scientific	Cat# Mm00514283_s1
Eef1a1 mouse TaqMan Primer	ThermoFisher Scientific	Cat# Mm01973893_g1
Software and algorithms		
Ingenuity Pathway Analysis	Qiagen	https://digitalinsights.qiagen.com/products-overview/discovery-insights-portfolio/analysis-and-visualization/qiagen-ipa/
Cell Ranger 3.0.2	10x Genomics	https://support.10xgenomics.com/single-cell-gene-expression/software/release-notes/3–0
Monocle (R environment)	Trapnell Lab	https://cole-trapnell-lab.github.io/monocle3/docs/introduction/
Seurat (R environment)	Satija Lab	https://satijalab.org/seurat/
Other		
45% Corn Oil Diet	Research Diets	Modified from base diet D12344

RESOURCE AVAILABILITY

Lead contact

Further information and requests for resources and reagents should be directed to and will be fulfilled by the lead contact, Michael Rudolph (michael-rudolph@ouhsc.edu).

Materials availability

This study did not generate new unique reagents.

Data and code availability

Bulk and single-cell RNA-seq data are deposited in GEO and are publicly available under accession number GSE155895.

This paper does not report original code.

Any additional information required to reanalyze the data reported in this paper is available from the lead contact upon request.

EXPERIMENTAL MODEL AND SUBJECT DETAILS

Mouse care

Animal procedures were approved by the IACUC and housed at the University of Colorado Anschutz Campus Vivarium. Wildtype C57BL/6J mice were purchased from Jackson Laboratories (Bar Harbor,

MN, USA). *Fat-1*mice were kindly provided by Dr. Kang and genotyped according to his protocol.[41] Heterozygous *fat-1* females were bred with wildtype males generating 50% wildtype offspring as described.[42] The study design used wildtype (WT, high n6/n3 ratio) and *fat-1* (low n6/n3 ratio) mothers to test PUFA ratio exposures in offspring development (Figure 1). Female mice were provided chow until the time of mating at 10 weeks old, at which time they were switched to 45% fat (corn oil) diet and underwent normal gestation and lactation. At postnatal day 12 (PND12), both WT and *fat-1* dams and their entire cross-fostered litters (males and females combined) were assessed for body composition, and pups were sacrificed for adipose morphology, cellularity, primary AP cell flow cytometry, gene expression, protein levels, and for circulating hormones, glucose, and fatty acid composition. Only cross-fostered WT offspring were used for downstream assays, and litters were standardized to 6–8 pups per dam. At PND5, dams were given 5% D_2O in their drinking water to provide deuterium tracer to the pups via their milk.

Model design

WT offspring from control gestation dams were cross-fostered onto either WT (high n6/n3) or *fat-1* (low n6/n3) dams that were provided 18:2 n6 rich diet (Figure 1). Specialized diet was provided to the dams as prepared by Research Diets, Inc., New Brunswick, NJ (D12344; 45% kCal fat from corn oil without sucrose, see also Data S1). All litters were considered mixed feed, as they were allowed to suckle *ad libitum*, and litter sacrifices took place between 8 a.m. and 12 p.m.

METHOD DETAILS

Body composition

Body composition was quantified by magnetic resonance (qMR; Echo MRI Whole Body Composition Analyzer; Echo Medical Systems, Houston, TX, USA) on PND12 for dams and their cross fostered litters.

Lipid and DNA gas chromatography-mass spectrometry

Total lipids were extracted and fatty acid profiles quantified by GC/MS. Briefly, 5 μL milk (thawed at 37°C and mixed by inversion) or 6 μL serum was added to 500 μL of potassium phosphate buffer pH 6.8. Then 10 μL (for plasma) or 40 μL (for milk) 1N HCl was added to this mixture and vortexed lightly. Then 500 μL of methanol was added and samples were vortexed vigorously. Total lipid extraction was performed using 3:1 (v/v) isooctane/ethyl acetate solution to extract the milk/plasma fat and the samples were resuspended in 300 μL of isooctane.

An appropriate amount of internal standards were added to 50 μL of isooctane-suspended total milk/serum lipid and evaporated to dryness, saponified with 100% Ethanol and 1N NaOH (500 μL each) at 90°C for 30 min and neutralized with 525 μL 1N HCl. Saponified fatty acids were then extracted twice with 1.5 mL Hexane, dried and derivatized with Pentafluorobenzyl bromide (PFBBr, 25 μL) in 25 μL of N,N-Diisopropylethylamine (DIEA) for 30 min at 37°C, dried again and resuspended in Hexane. 1 μL of this Hexane suspension was run on Agilent 8890 GC and 5977B MS to quantify the amounts of total fatty acids present in milk or serum.[15,82] Total serum protein was measured by BCA assay. Data are expressed in μmoles of fatty acid per mL of milk or mg of total serum protein. The total n6/n3 PUFA ratio is the quantitative sum of n6 divided by the sum of n3 PUFA; the AA/DHA+EPA ratio is the μmoles of 20:4 n6 divided by the 22:6 n3 + 20:5 n3; the LA/LNA ratio is the μmoles of 18:2 n6 (LA) divided by 18:3 n3 (LNA). DNA was isolated from primary adipocyte progenitors (Sca1+/CD24+), preadipocytes (Sca1+/CD24-), SWAT, and whole blood cells using the ZR-Duet MiniPrep Plus Kit according to the manufacturer's protocol (Zymogen Research). The incorporation of deuterium into DNA to quantify *in vivo* proliferation was adapted from Busch et al.[54,55] and Foletta et al.[53] Extracted DNA concentration was quantified by Qubit 3.0 fluorometric measurement (ThermoFisher). Briefly, 30 ng of total DNA was input into each hydrolysis reaction containing 200 μL of 1x hydrolysis buffer + 50 μL of 5x enzyme mix (5x hydrolysis buffer containing S1nuclease [Sigma; N5661; 50 kU] and potato acid phosphatase [Merck Millipore/Calbiochem; 524529; 1 kU] according to Foletta et al.,[53] DNA was hydrolyzed overnight at 37°C in a shaking water bath (150 RPM), spun down, 5 ng of uniformly labeled ^{13}C-deoxyribose and was added, and samples were snap-frozen until derivatization. The samples were acidified by the addition of 10 μL of 0.2M HCl to the hydrolyzed sample, vortexed vigorously, and collected. 10 μL of 50 mM O-(2,3,4,5,6-pentafluorobenzyl) hydroxylamine hydrochloride (PFHBA, 12.5 mg/mL H_2O stock solution) was added, and samples were mixed by vortexing, transferred to 12 × 75-mm screw-cap tubes (Kimble), and incubated at 95°C for 1 h. The oxime of deoxyribose was extracted by the addition of 100 μL of 5 M NaCl, vortexed, followed by 1 mL of 2:1 (v/v) hexane/ethyl acetate

and vigorous vortexing for 20 s. Samples were allowed to sit for 5 min at RT, centrifuged at 1000 xG for 2 min, and the organic phase was transferred to new 12 × 75-mm screw cap tubes. The aqueous fraction was re-extracted with 1 mL of 2:1 (v/v) hexane/ethyl acetate as above, the organic phase was combined with the initial extraction, and samples were taken to dryness by speed-vac (no heat). Dried samples were resuspended in 25 μL of acetonitrile, and free hydroxyl groups were trimethylsilylated with 25 μL N,O-Bis (trimethylsilyl)trifluoroacetamide (BSTFA, Sigma Aldrich), incubated at 60°C for 45 min, spun down, and transferred to GC/MS autosampler vials. Samples were taken to dryness, resuspended in 40 μL of 100% hexane, and 1 μL was injected to quantify the molar enrichment of the M + 1 ion.

Flow cytometry sorting and analysis

Subcutaneous adipose tissue was minced and digested in Hanks Balanced Salt Solution (HBSS) (Sigma, H8264) containing 3% BSA, 0.8 mg mL^{-1} collagenase type 2 (Worthington Biochemical, LS004174), 0.8 mM $ZnCl_2$, 1.0 mM $MgCl_2$ and 1.2 mM $CaCl_2$ for 45 min at 37°C in an orbital shaker at 150 RPM, and samples were shaken vigorously by hand for 1 min after digestion. The resulting solution was then filtered through a 70 μm filter. Cells in the stromal vasculature fraction were pelleted at 300 xG, washed with HBSS buffer containing 3% BSA, and stained with primary antibodies on ice for 30 min. The following antibodies were used: CD45 FITC at 1:1,000 (BioLegend; 103108), CD31 PE-Cy7 at 1:500 (BioLegend, 102417), CD29 Alexa Fluor 700 at 1:200 (BioLegend, 102218), CD34 APC at 1:50 (BioLegend, 119310), Sca-1 BV510 at 1:200 (BioLegend, 108129), and CD24 PE at 1:100 (BioLegend, 138504). Following antibody incubation, cells were washed with their respective buffers, and unfixed cell preparations were treated with DAPI (Invitrogen) at 1ug/mL to exclude dead cells. Cells were sorted using a FACS Aria Fusion equipped with FACS DiVA software (BD Biosciences). Cell populations were selected based on forward scatter (FSC) and side scatter (SSC), and dead cells that had taken up DAPI were excluded. Single cells were isolated or analyzed based on cell surface markers.[56] Data was analyzed using BD FACS DiVA and FlowJo.

Seahorse cellular metabolic assays

Seahorse substrate oxidation assays were carried out using manufacturer's instructions with some modifications, utilizing the glucose/pyruvate oxidation stress test kit (103673-100), glutamine oxidation stress test kit (103674-100), and palmitate oxidation stress test kit (103693-100). Modifications include adding 20 μL inhibitors per well directly to the cells 15 min before the assay, and then following the standard mitochondrial stress test protocol for the assay. For each seahorse assay, 30,0000 flow-sorted Sca-1+ APCs were seeded per well. Flow-sorted APCs from three independent dam/litter dyads for each condition (low and high n6/n3) were plated for Seahorse assays. Each SVF was prepared from a litter of 6–8 pups, including both males and females. Since these are primary cells, the initial seeding density was higher than normally used in Seahorse plates, because some loss of cells was expected after seeding. The seahorse plates were not coated and used as is for culturing primary cells. For all seahorse assays, the concentrations of Oligomycin, FCCP and Rotenone/Antimycin used were 1.5 , 2 and 0.5 μM, respectively. The inhibitors Etomoxir, UK5009 and BPTES were used at concentrations of 4 , 2 and 3 μM, respectively. The data were normalized with cell number as measured using Sulforhodamine B colorimetric assay.

Tissue culture of mouse APC cell line EVC005

The immortalized adipocyte precursor cell line was purchased from Kerafest, MA, USA (EVC005, kerafest.com). Cells were cultured in Dulbecco's Modified Eagle Medium (DMEM) containing 10% fetal bovine serum (FBS) supplemented with penicillin (100 U/mL) and streptomycin (100 μg/mL) at 37°C in a humidified incubator with 5% CO_2. One day before treatment with 1-DSO-BSA conjugate (NR2F2 ligand), 2×10^5 cells were seeded per well of a 6-well plate and incubated overnight. APCs were then treated with 1-DSO-BSA conjugate (300 nM) for 48h, control cells were treated with only BSA (vehicle). Purified 1-Deoxysphingosine (m18:1(14Z)) (1-DSO) was purchased from Cayman Chemical, Ann Arbor, MI, and 1-deoxysphingolipid-BSA complexes were prepared. Briefly, 2 mM 1-DSO stock solution was prepared in 100% ethanol by mixing 57 μL of 1-DSO stock (3.5 mM) with 43 μL 100% ethanol. A 100 μM 1-DSO-BSA conjugate solution was then prepared by adding 50 μL of 2 mM 1-DSO stock to 100 μM fatty acid-free BSA in PBS containing 10 mM HEPES, and the final working concentration of 1-DSO-BSA conjugate was 300 nM.[58]

qPCR for mouse APC cell line EVC005

Total RNA was extracted using the RNeasy Plus Mini Kit (Qiagen, Hilden, Germany, 74134) according to the manufacturer's protocol, and 200 ng of total RNA was reverse transcribed into cDNA using iScript Reverse

Transcription Supermix (Bio-Rad, Hercules, CA, USA, 1708841). cDNA representing 25 ng of total RNA was added to each qPCR reaction containing TaqMan master mix and primers (ThermoFisher, MA, USA) specific for Prdm16, P2rx5, Runx1, Ucp2, Dnmt1, Pparγ2 and C/ebpα were used for quantitative real-time PCR (Applied Biosystem, Ca, USA). Eef1a1 was included as a housekeeping gene.

Live cell TMRE staining

EVC005 cells were cultured and treated with 1DSO-BSA conjugate as described above. Following 48 h, the media were changed to fresh DMEM containing 1 μM tetramethylrhodamine ethyl ester (TMRE, Biotium) live cell mitochondrial potential dye. Cells were incubated with TMRE at 37°C for 15 min before fluorescent data was collected using Zoe™ Fluorescent Cell Imager (BioRad).

Simple Western using JESS

Flow-sorted $CD34^+$, $CD29^+$, Sca-1+ primary APCs and EVC005 cells (treated with or without 1DSO) were homogenized in RIPA buffer with protease and phosphatase inhibitors. Lysates from primary APCs were run on ProteinSimple JESS instrument for UCP2 (Cell Signaling, 89326), CEPBa (Cell Signaling, 8178), NR2F2 (Cell Signaling, 6434) and DNMT1 (Novus Biologicals, NB100-56519) antibodies. The antibodies used while running the EVC005 lysate were TOM20 (Cell Signaling, 42406), SOD2 (Cell Signaling, 13141), NRF1 (Cell Signaling 46743), HSP90 (Cell Signaling, 4874), OxPhos Rodent WB Antibody cocktail (ThermoFisher, 45–8099) and GAPDH (Cell Signaling, 5174). All antibodies were used at a dilution of 1/50 for JESS westerns. Three microliters of 1.2 mg/mL protein was loaded per well for the JESS assays. Proteins from primary APCs from 6 different SVFs for each condition (high or low n6/n3) were used for each JESS assay.

Total RNA/DNA isolation and RNA sequencing library preparation

Total RNA and DNA were isolated from primary adipocyte progenitor (Sca1+/CD24+) and preadipocyte (Sca1+/CD24-) cells using the ZR-Duet MiniPrep Plus Kit according to the manufacturer's instruction (Zymogen Research). Total DNA (used for D_2O incorporation assay) and RNA integrity were assessed for quality using the Agilent 4200 Tape Station. RNA-seq library construction was completed using 200 ng of total RNA according to the Nugen Universal Plus mRNA-SEQ instructions (kit #0508). Sequencing was performed on the Illumina HiSEQ 6000 instrument using single 50 base pair reads. The average reads/bases quality for all the samples in the lanes is at least 97% ≥ Q30. The filtered reads distribution for all the samples/barcodes across the lanes ranged from approx 9M–44M single-end reads.

Bulk and single-cell RNA-seq data processing and mRNA profiling

All raw sequencing files may be obtained using GEO id: GSE155895 (https://www.ncbi.nlm.nih.gov/geo/). Using the Duet DNA/RNA extraction kit (Zymogen Research), flow-sorted $CD24^+$ progenitor and $CD24^-$ preadipocyte APCs (Lin-, $CD29^+$, $CD34^+$, Sca-1+) were lysed and total RNA was isolated according to manufacturer protocol. Total RNA quantity was measured by NanoDrop (ThermoFisher), and RNA quality was assessed by Agilent Tape Station 4200 (Agilent, Santa Clara, CA). 100 ng of total RNA was used as input to construct sequencing libraries using the Universal Plus mRNA-SEQ kit according to manufacturer protocol (NuGEN, Redwood City, CA) and sequencing data were collected with an Illumina HiSEQ4000 using 1 × 50 single read sequencing (Illumina, San Diego, CA) by the University of Colorado Cancer Center Genomics and Microarray core facility.

Bulk RNA-sequencing

Sequenced reads were trimmed, aligned, and a raw counts matrix of all genes was generated using Salmon (Mouse Release M23) and imported into R using the tximport package, and DESeq2 (DESeq2 version 1.30.1) in R was used to normalize, Log2 transform, and calculate significantly different genes.[83] Log2 transformed and significantly different gene lists were analyzed using IPA (QIAGEN Inc., www.qiagenbioinformatics.com).

scRNA-sequencing

Flow-sorted Sca1+ APCs were counted using a hemocytometer, and ~4,000 cells per n6/n3 PUFA ratio group were captured using the 10x Genomics Chromium platform and reagents according to the manufacturer's instructions. Fastq files for each sample were processed using Cell Ranger 3.0.2 (10x Genomics) with mm10 as the reference genome. A total of 6,905 cells (High n6/n3, n = 3,321; Low n6/n3, n = 3,584)

remained following aggregation, with an average of 106,425 reads per cell (High n6/n3 PUFA, 110,325 reads per cell; Low n6/n3 PUFA, 102,810 reads per cell). Data were filtered, normalized, scaled, and analyzed using Seurat v3.0.2 (SatijaLab) in an R v3.5.1 environment. Briefly, the raw Cellranger sparse matrix was imported into Seurat, cells with unique gene counts <500 or mitochondrial percentages >30% resulted in 6,811 cells in the final analysis, with an average of 12,630 UMI counts per cell and a median of 2,967 genes per cell, and the sparse matrix was converted into a Seurat object to generate clusters and calculate differential genes within a cluster by PUFA treatment.[84]

Pseudotime analysis

Cell data were formatted for use with Monocle3 v0.1.1 from Seurat within R. A new UMAP was generated using the default protocol shown on the Monocle3 Website (https://cole-trapnell-lab.github.io/monocle3/docs/introduction/), using 9 principal components again as the input. Pseudotime was calculated using all partitions to facilitate the identification of progenitor cells. The resulting pseudotime was stored in the Seurat object to view in the original UMAP space. Pearson correlation was used to identify genes with a linear relationship to pseudotime.

Offspring plasma proteomics

From 50 μL plasma, serum albumin, Ig, fibrinogen, transferrin, IgM, haptoglobin, and alpha1-antitrypsin were removed using Seppro® Mouse columns according to manufacturer's protocol (Sigma-Aldrich), and depleted plasma was digested according to the FASP protocol using a 30 kDa molecular weight cutoff filter. Briefly, samples were mixed in the filter unit with 8M urea in 0.1M ammonium bicarbonate pH 8.5 buffer (ABCB), centrifuged at 14 000g for 15 min, and proteins were reduced by the addition of 100 μL of 10 mM DTT in 8M urea in 0.1M ABCB for 30 min at RT and the device was centrifuged. Subsequently, 100 μL of 55 mM iodoacetamide in 8M urea in ABCB was added to the samples, incubated for 30 min at RT in the dark, and collected by centrifugation. Samples were washed three times with 100 μL of 8M urea in ABCB, followed by three washes with 100 μL of 0.1M ammonium bicarbonate pH 8.5 buffer. Proteins were digested using 0.02% of ProteaseMax (Promega, Madison, WI) detergent at 37°C overnight. Peptides were recovered by transferring the filter unit to a new collection tube and spinning at 14 000g for 10 min. To complete peptide recovery, we rinsed filters twice with 50 μL of 0.2% FA and 10 mM ABC that was collected by centrifugation. The peptide mixture was desalted and concentrated on Thermo Scientific Pierce C18 Tip.

Database searching, protein identification. Samples were analyzed on a Q Exactive HF quadrupole orbitrap mass spectrometer (Thermo Fisher Scientific, Waltham, MA, USA) coupled to an Easy nLC 1000 UHPLC (Thermo Fisher Scientific) through a nanoelectrospray ion source. Peptides were separated on a self-made C18 analytical column (100 μm internal diameter x 20 cm length) packed with 2.7 μm Phenomenex Cortecs particles. The peptides were separated by a 180 min linear gradient from 4% to 30% acetonitrile at 400 nL/min using 0.1% formic acid in water (Buffer A) and 0.1% formic acid in acetonitrile (Buffer B) (Optima LC/MS, Fisher Scientific, Pittsburgh, PA). Mass spectra were acquired using Xcalibur software (version 4.0) in positive ion mode, and full MS scans ranged from *m/z* 300 to 1600 with a mass resolution of 120,000 at m/z 200 and a target value of 1.00E+06 with a maximum injection time of 50 ms. Precursor ions with single, unassigned, or eight and higher charge states from fragmentation selection were excluded. MS/MS spectra were extracted from raw data files, converted into mgf files using a PAVA script (UCSF, MSF, San Francisco, CA), and were queried against mouse SwissProt database using Mascot (ver 2.2.06, Matrix Science) using mass tolerances of +/− 10 ppm for MS peaks, and +/− 20 ppm for MS/MS fragment ions. Trypsin specificity was used allowing for 1 missed cleavage. Scaf-fold (ver 4.4.0, Proteome Software, Portland, OR, USA) was used to validate MS/MS-based peptide and protein identifications. Peptides were accepted at > 95.0% probability specified by the Peptide Prophet algorithm, and protein identifications were accepted at > 99.0% probability containing at least two identified unique peptides.

Enzyme-linked immunosorbent assay

ELISA for high molecular weight (HMW) and total adiponectin (ALPCO, 47-ADPMS-E01), Acylation Stimulating Protein (ASP, MyBioSource, MBS263213), Complement C3 (Abcam, ab157711), Insulin (Crystal Chem, 90080), Leptin (R&D, DY498) and Retinol-Binding Protein 4 (RBP4, R&D, DY3476) were performed following manufacturers' instructions. Pup serum was collected from trunk blood (pooled from 2 to 3 pups per group) and diluted 1:8181, 1:200, 1:50000, 1:1, 1:1, and 1:2000 for HMW and total adiponectin, ASP, Complement C3, Insulin, Leptin, and RBP4, respectively.

QUANTIFICATION AND STATISTICAL ANALYSES

The n per n6/n3 exposure group was the number of independent WT or *fat-1* dams nursing the cross-fostered WT litters unless otherwise noted. All statistics were calculated by ANOVA in the respective software packages as described above, except the proteomics data that used a Fisher Exact test within the Scaf-fold proteomics software between n6/n3 exposure groups (ver 4.4.0, Proteome Software, Portland, OR, USA), the scRNA sequencing data in which differentially expressed genes between the high- and low-n6/n3 groups were obtained for each cluster using Student's t-test. Adjusted p values were generated using a Bonferroni correction and a cutoff was set at adj. p value ≤ 0.05, and the adipocyte cellularity data used a Kolmogrov-Smirnov test that compares the cumulative distributions between n6/n3 FA exposure groups.